NOAA Technical Report NESS 84

Use of NOAA/AVHRR Visible and Near-Infrared Data for Land Remote Sensing

Washington, D.C.
September 1981

U.S. DEPARTMENT OF COMMERCE
National Oceanic and Atmospheric Administration
National Earth Satellite Service

NOAA TECHNICAL REPORTS

National Environmental Satellite Service Series

The National Environmental Satellite Service (NESS) is responsible for the establishment and operation of the environmental satellite systems of NOAA.

Publication of a report in NOAA Technical Report NESS series will not preclude later publication in an expanded or modified form in scientific journals. NESS series of NOAA Technical Reports is a continuation of, and retains the consecutive numbering sequence of, the former series, ESSA Technical Report National Environmental Satellite Center (NESC), and of the earlier series, Weather Bureau Meteorological Satellite Laboratory (MSL) Report. Reports 1 through 39 are listed in publication NESC 56 of this series.

Reports in the series are available from the National Technical Information Service (NTIS), U.S. Department of Commerce, Sills Bldg., 5285 Port Royal Road, Springfield, VA 22161, in paper copy or microfiche form. Order by accession number, when given, in parentheses. Beginning with 64, printed copies of the reports, if available, can be ordered through the Superintendent of Documents, U.S. Government Printing Office, Washington, DC 20402. Prices given on request from the Superintendent of Documents or NTIS.

ESSA Technical Reports

NESC 46 Monthly and Seasonal Mean Global Charts of Brightness From ESSA 3 and ESSA 5 Digitized Pictures, February 1967-February 1968. V. Ray Taylor and Jay S. Winston, November 1968, 9 pp. plus 17 charts. (PB-180-717)

NESC 47 A Polynomial Representation of Carbon Dioxide and Water Vapor Transmission. William L. Smith, February 1969 (reprinted April 1971), 20 pp. (PB-183-296)

NESC 48 Statistical Estimation of the Atmosphere's Geopotential Height Distribution From Satellite Radiation Measurements. William L. Smith, February 1969, 29 pp. (PB-183-297)

NESC 49 Synoptic/Dynamic Diagnosis of a Developing Low-Level Cyclone and Its Satellite-Viewed Cloud Patterns. Harold J. Brodrick and E. Paul McClain, May 1969, 26 pp. (PB-184-612)

NESC 50 Estimating Maximum Wind Speed of Tropical Storms From High Resolution Infrared Data. L. F. Hubert, A. Timchalk, and S. Fritz, May 1969, 33 pp. (PB-184-611)

NESC 51 Application of Meteorological Satellite Data in Analysis and Forecasting. Ralph K. Anderson, Jerome P. Ashman, Fred Bittner, Golden R. Farr, Edward W. Ferguson, Vincent J. Oliver, Arthur H. Smith, James F. W. Purdom, and Rance W. Skidmore, March 1974 (reprint and revision of NESC 51, September 1969, and inclusion of Supplement, November 1971, and Supplement 2, March 1973), pp. 1--6C-18 plus references.

NESC 52 Data Reduction Processes for Spinning Flat-Plate Satellite-Borne Radiometers. Torrence H. MacDonald, July 1970, 37 pp. (COM-71-00132)

NESC 53 Archiving and Climatological Applications of Meteorological Satellite Data. John A. Leese, Arthur L. Booth, and Frederick A. Godshall, July 1970, pp. 1-1--5-8 plus references and appendixes A through D. (COM-71-00076)

NESC 54 Estimating Cloud Amount and Height From Satellite Infrared Radiation Data. P. Krishna Rao, July 1970, 11 pp. (PB-194-685)

NESC 56 Time-Longitude Sections of Tropical Cloudiness (December 1966-November 1967). J. M. Wallace, July 1970, 37 pp. (COM-71-00131)

NOAA Technical Reports

NESS 55 The Use of Satellite-Observed Cloud Patterns in Northern Hemisphere 500-mb Numerical Analysis. Roland E. Nagle and Christopher M. Hayden, April 1971, 25 pp. plus appendixes A, B, and C. (COM-73-50262)

NESS 57 Table of Scattering Function of Infrared Radiation for Water Clouds. Giichi Yamamoto, Masayuki Tanaka, and Shoji Asano, April 1971, 8 pp. plus tables. (COM-71-50312)

NESS 58 The Airborne ITPR Brassboard Experiment. W. L. Smith, D. T. Hilleary, E. C. Baldwin, W. Jacob, H. Jacobowitz, G. Nelson, S. Soules, and D. Q. Wark, March 1972, 74 pp. (COM-72-10557)

NESS 59 Temperature Sounding From Satellites. S. Fritz, D. Q. Wark, H. E. Fleming, W. L. Smith, H. Jacobowitz, D. T. Hilleary, and J. C. Alishouse, July 1972, 49 pp. (COM-72-50963)

NESS 60 Satellite Measurements of Aerosol Backscattered Radiation From the Nimbus F Earth Radiation Budget Experiment. H. Jacobowitz, W. L. Smith, and A. J. Drummond, August 1972, 9 pp. (COM-72-51031)

(Continued on inside back cover)

NOAA Technical Report NESS 84

Use of NOAA/AVHRR Visible and Near-Infrared Data for Land Remote Sensing

Stanley R. Schneider
David F. McGinnis Jr.
James A. Gatlin

Washington, D.C.
September 1981

U.S. DEPARTMENT OF COMMERCE
Malcolm Baldrige, Secretary

National Oceanic and Atmospheric Administration
John V. Byrne, Administrator

National Earth Satellite Service
David S. Johnson, Assistant Administrator

CONTENTS

Use of NOAA/AVHRR Visible and Near-Infrared Data
For Land Remote Sensing

Stanley R. Schneider[1], David F. McGinnis Jr.[1]
and James A. Gatlin[2]

Abstract

NOAA-6 AVHRR visible and near-infrared digital data were analyzed for their usefulness in monitoring lake ice, snowcover, water quality, crop condition and terrain classification on the H.P. 1000 computer interactive system. Terrain phenomena that had heretofore been studied using Landsat MSS data could also be monitored with the NOAA-6 channels, but at a lesser resolution.

[1]Hydrologists, NOAA/National Earth Satellite Service, Dept. of Commerce, Washington, D.C.

[2]Chief, Sensor Evaluation Branch, NASA Goddard Space Flight Center, Greenbelt, MD.

INTRODUCTION

On July 23, 1972, the National Aeronautics and Space Administration (NASA) launched the Earth Resources Technology Satellite, later renamed Landsat-1. Two follow-up satellites in the series, Landsats-2 and -3 were launched in January 1975 and March 1978 respectively. Each of these satellites contains a Multispectral Scanner (MSS) which provides 80 meter resolution coverage in four different spectral channels. Of particular interest to this study are the visible (MSS band 5) and near infrared, (MSS band 7) channels. Data from these channels have been demonstrated to be useful in studies of lake ice, snowcover, water quality, crop growth and terrain classification (Short et al., 1976.)

In October 1978, the National Oceanic and Atmospheric Administration/National Earth Satellite Service (NOAA/NESS) launched TIROS-N the first operational four channel polar orbiting satellite. Previous NOAA polar orbiting satellites (the ITOS series) had contained sensors that imaged only in the visible and thermal infrared regions of the spectrum. The Advanced Very High Resolution Radiometer (AVHRR) onboard TIROS-N provided data in the four spectral intervals of: 0.55-0.9 um, 0.725-1.1 um, 3.55-3.93 um and 10.5-11.5 um. Because the overlap in the first two channels hindered effective multispectral studies it was decided that future satellites in the series would have AVHRRs with the first channel narrowed to the purely visible region ie, 0.58-0.68 um. This adjustment became effective with the launch of NOAA-6 in June 1979. Figure 1 shows spectral response curves for MSS bands 5 and 7 and NOAA-6 AVHRR channel 1 and 2. Although the curves are quite similar, note that the AVHRR channel 2 responds to energy from a larger portion of the spectrum than MSS band 7. Whereas the MSS band 7 response begins at about 0.8 um, almost 30 percent of the AVHRR channel 2 response lies in the 0.7 um to 0.8 um region. The purpose of this report is to assess the comparative usefulness of NOAA-6 AVHRR channels 1 and 2 in the monitoring of terrain phenomena that have been previously studied using Landsat MSS data.

SATELLITE, SENSOR AND DATA

The NOAA-6 satellite operates at an altitude of 850 km with a local equatorial crossing time of 0730 and 1930. It has an orbital period of 102 minutes which produces 14.1 orbits per day. Its four channel AVHRR has an instantaneous field of view (IFOV) of 1.4 milliradians which yields a resolution of 1.1 km. NOAA-6 scans the earth spanning an angle $\pm$56 degrees from nadir.

AVHRR data used in this study were originally ingested onto a tape recorder onboard the NOAA-6 satellite and transmitted to the NESS Command and Data Acquisition (CDA) station at Wallops Island, Virginia. From there the data were retransmitted via a communications satellite to NESS headquarters in Suitland, Maryland, for permanent storage on a Terra Bit Memory, (TBM) system. The data were then dumped to nine-track computer compatible tapes (CCT's) for detailed study and analysis. Tapes were generated for the following three (3) cases:

Date	Orbit #
12 April 80	4123
27 April 80	4322
4 May 80	4436

Tapes for each orbit contain 11 minutes of data covering an earth swath of 4500 km (along the orbital track) x 2700 km (horizon-to-horizon). Each recorded satellite pass consists of about 4000 scan lines; each scan line is comprised in turn of 2048 picture elements (pixels). These data pixels are represented on the tapes as 10 bit digital counts with values ranging from 0 to 1023. Calibration coefficients, solar zenith angles and earth location data are included with each scan line. Coefficients used to convert AVHRR channels 1 and 2 digital counts into planetary albedoes were developed during pre-launch calibration tests. Look-up tables consisting of 8-bit count-to-albedo relationships for both channels 1 and 2 are given in Appendix A. Detailed information on NOAA-6 and the AVHRR can be found in Hussey (1977), Kidwell (1979) and Schwalb (1979).

DATA ANALYSIS METHODS

The AVHRR digital tapes were analyzed on the H.P. 1000 interactive system located at the NASA/Goddard Space Flight Center. A schematic of this system is included in Appendix B. Data may be displayed on this system with grid overlays and mapped to several different projections; gray shade and color enhancement capability is provided. A color bar of up to 64 levels can be selected from a possible 2048 different colors. Linear modification of image data can be performed on-line in the form of contouring the image, difference of two images, ratio of two images, differentiation of an image and combinations of these capabilities. A selected portion of an image may be enlarged or compressed by a floating point factor such as 2.2 or 3.0. On-line filtering and enhancement techniques are selectable. The methods available are median, laplacian, triangular convolution and gaussian convolution. Profiles of the image data may be obtained by horizontal, vertical, radial or circular sampling of the pixels. Hardcopy output is available by means of a plotting device and a video camera system. The camera uses Polaroid 8x10 color film which can be exposed and developed in less than two minutes for any selected image.

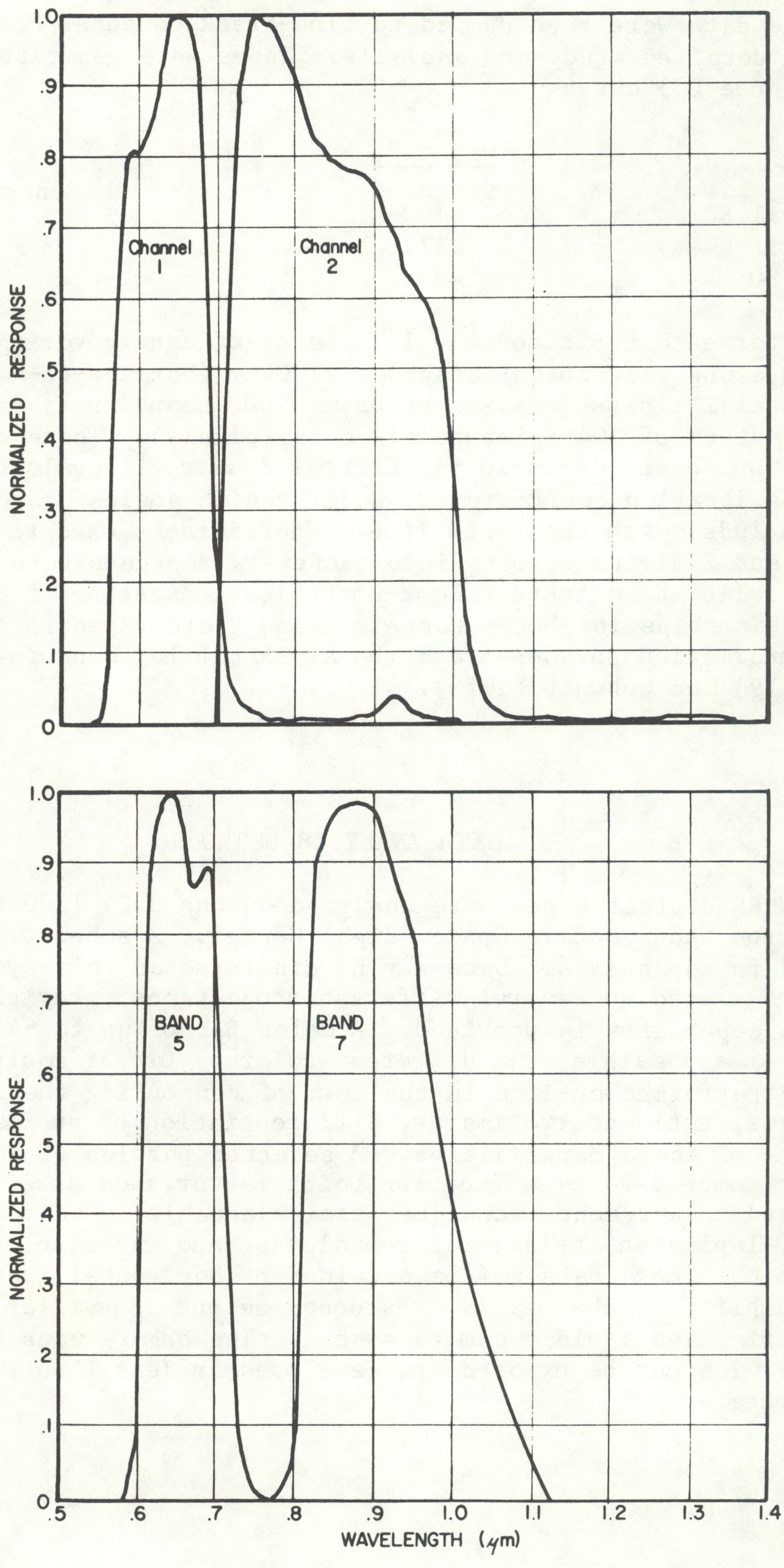

Figure 1 - Spectral response curves for NOAA-6 AVHRR channels 1 and 2, top. Response curves for Landsat MSS Bands 5 and 7, bottom.

CASE STUDIES

Lake Ice

Comparisons of visible and near-infrared satellite data for monitoring of lake ice was first documented by D.F. McGinnis (1972). Data from sensors onboard NASA's experimental Nimbus 3 meteorological satellite, launched in April 1969, were used in a study of four lakes in Canada: Winnipeg, Athabaska, Great Slave and Great Bear. It was found that "graduated melting conditions were detectable from the early stages to complete surface melt." Decreased reflectivity of ice in the near infrared has also been documented by Wiesnet et al (1974) in studies of Lake Erie ice using Landsat MSS bands 5 and 7 data.

For this study, lake ice was analyzed from NOAA-6 AVHRR data collected over Canada on April 12 and April 27, 1980. Local satellite overpass times wer 7:59 a.m. and 7:53 a.m. respectively.

Visible and near-infrared images of Lake Winnipeg, Manitoba are shown in Figures 2 (April 12) and 3 (April 27). On April 12 the lake, especially the northern section, appears bright in both the visible and near-infrared, due to a deep snowcover. The surrounding forest is partly snowcovered. On April 27 the lake appears darker in both spectral bands; in fact the southern part almost disappears in the near-infrared. The terrain east and west of the lake is snow-free on this latter date.

Figures 4 and 5 show "albedo" traces across transects labelled A-A and B-B in Figures 2 and 3. The digital count values were converted to albedoes using the satellite pre-launch calibrations and were normalized for varying illumination by dividing by cosine of the solar zenith angle. As used here, albedo is defined as the ratio of total solar radient energy returned by a body to the total solar radient energy incident on a body.

The April 12 plot in Figure 4 begins just west of the lake in snow-covered forest; here visible albedoes are in the 0.15 range. Visible albedoes over the lake exceed 0.80 and peak at 0.88. Near-infrared albedoes are 0.65-0.72 and are generally 0.15-0.17 less than the visible. The plots dip sharply near the western end of the profiles where the scan line crosses Selkirk Island. On April 27 the visible albedoes in Figure 4 have dropped to the 0.50-0.55 range, while near-infrared albedoes are 0.37-0.40. Note also that the profiles on April 27 are much noisier than those of two weeks earlier. By April 27 much of the snow may have melted away; the variations in albedo are likely due to variations in snow/ice thickness.

Figure 5 shows visible and near-infrared albedoes across southern Lake Winnipeg, along the line B-B in Figures 2 and 3. On April 12 visible albedoes are 0.80-0.83, while those in the near-infrared are 0.62-0.65. The sharp dip near the eastern shore represents Elk Island. Albedoes on the 27th are dramatically decreased: 0.21-0.23 for the visible, 0.16-0.19 for the near-infrared. In the near-infrared, the albedo of the snow-free forest adjacent

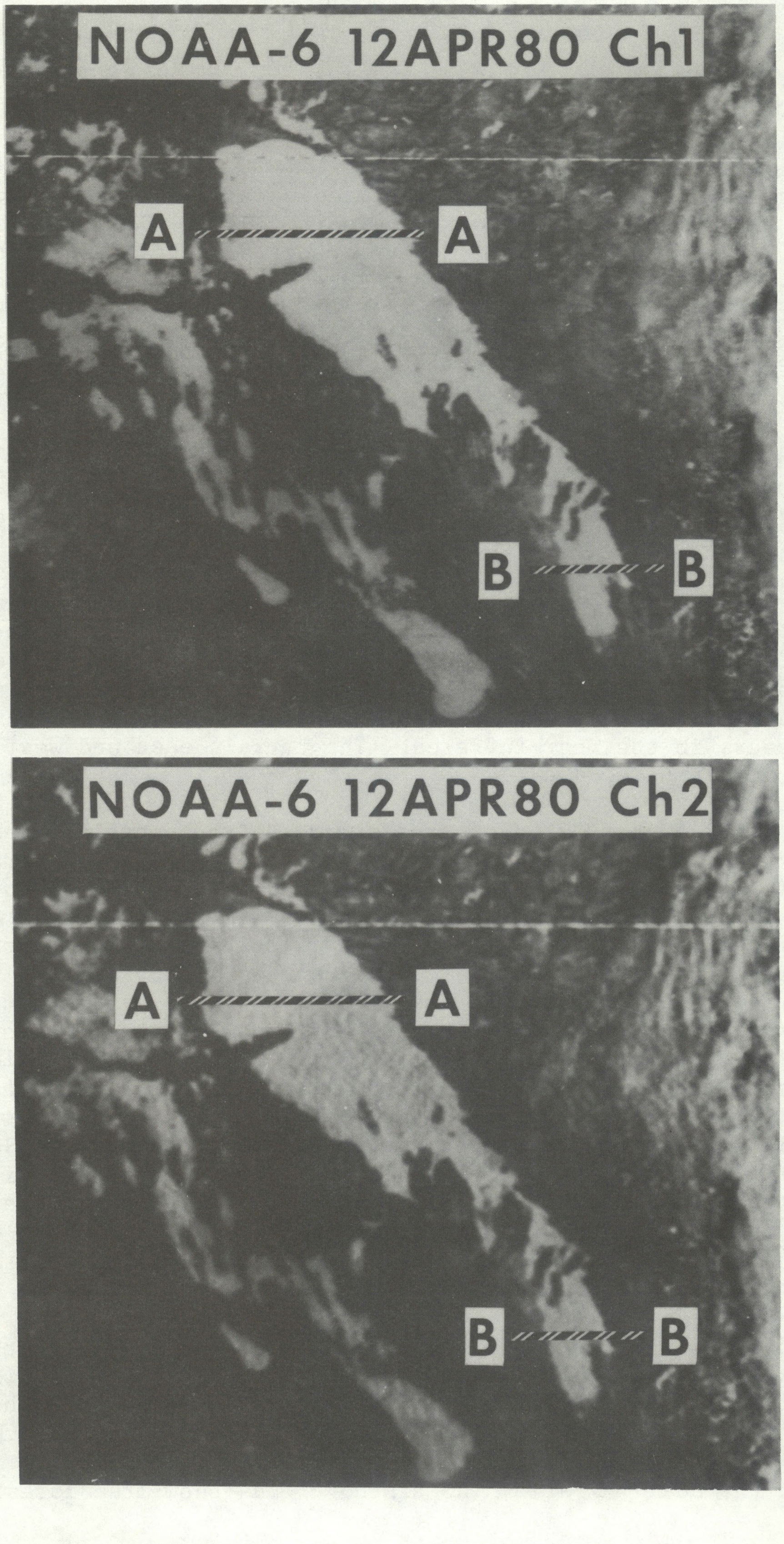

Figure 2 - Visible (top) and near-infrared (bottom) images of Lake Winnipeg on April 12, 1980, at 7:59 a.m. local time.

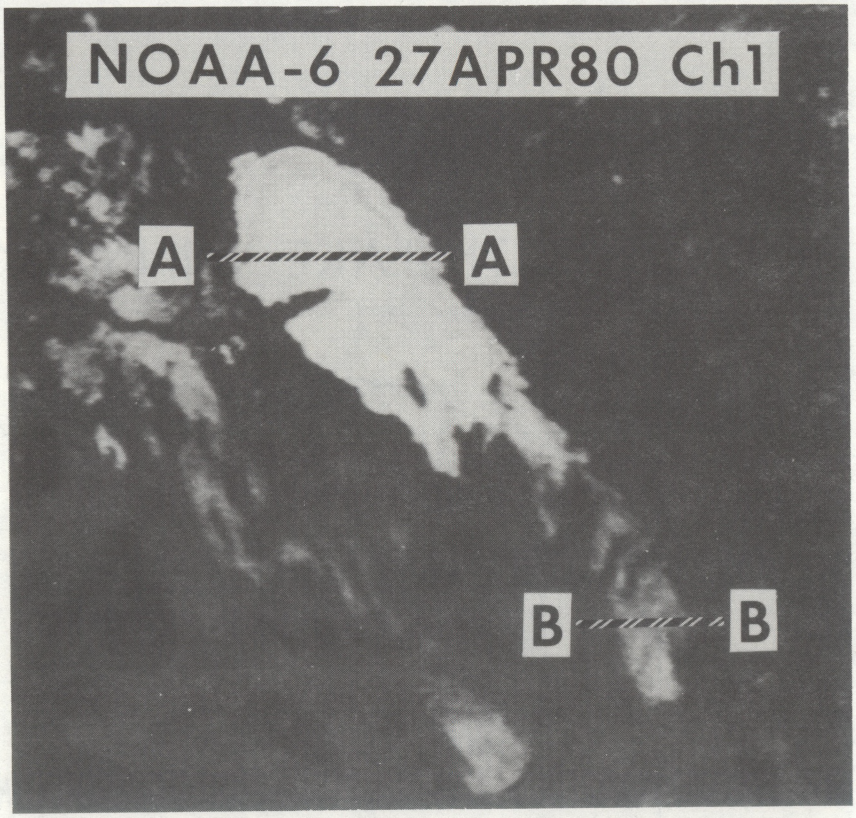

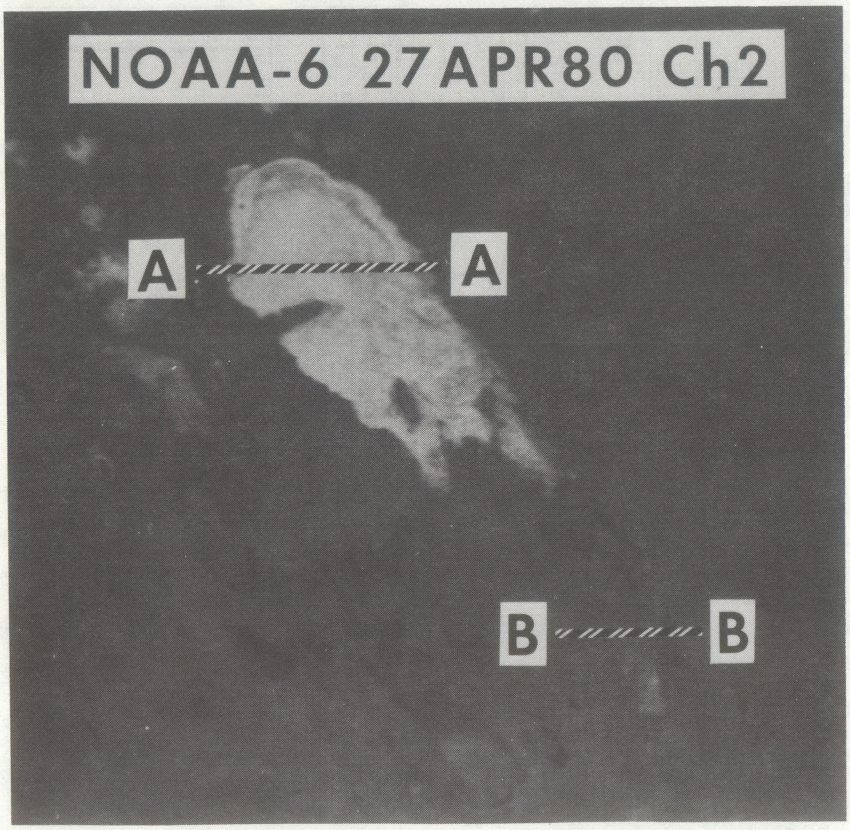

Figure 3 - Visible (top) and near-infrared (bottom) images of Lake Winnipeg on April 27, 1980, at 7:53 a.m. local time.

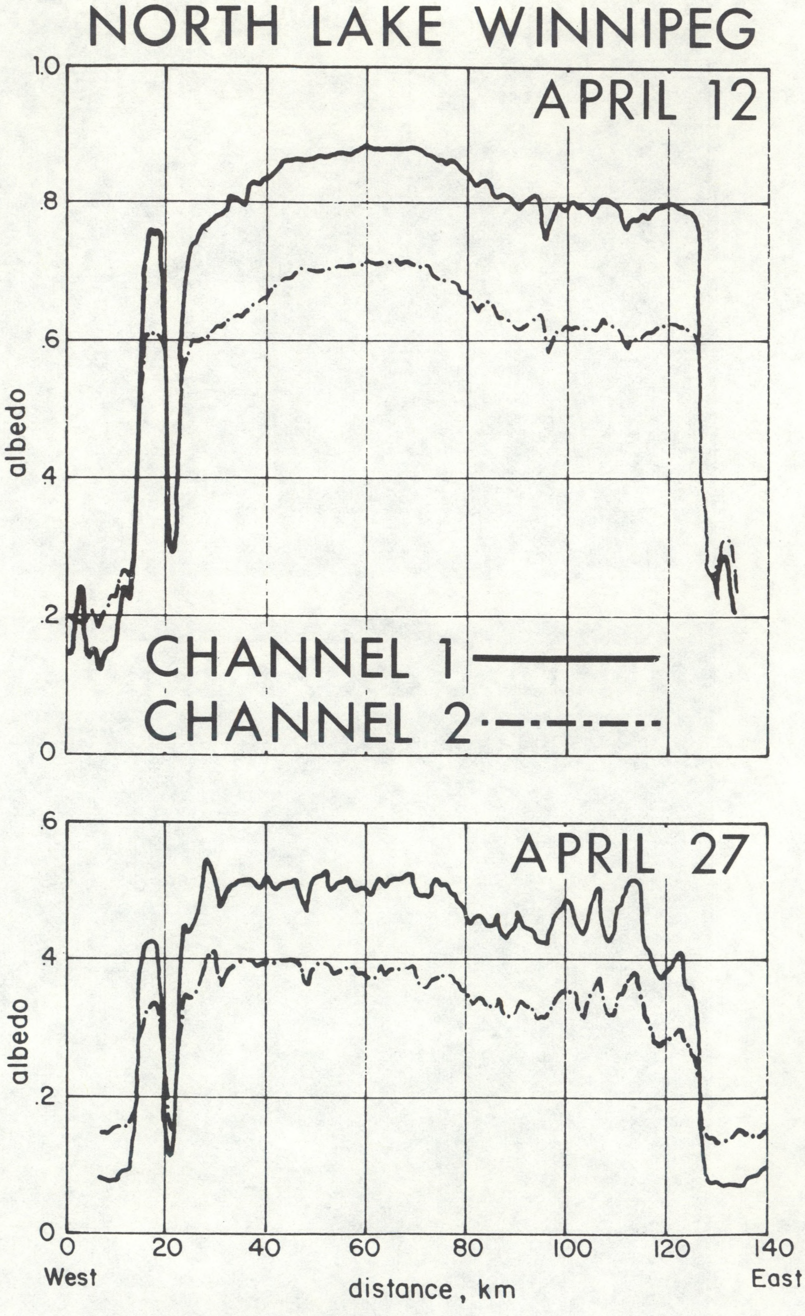

Figure 4 - Albedo trace (A-A on Figures 2 and 3) across northern Lake Winnipeg on April 12, 1980 (top) and April 27 (bottom).

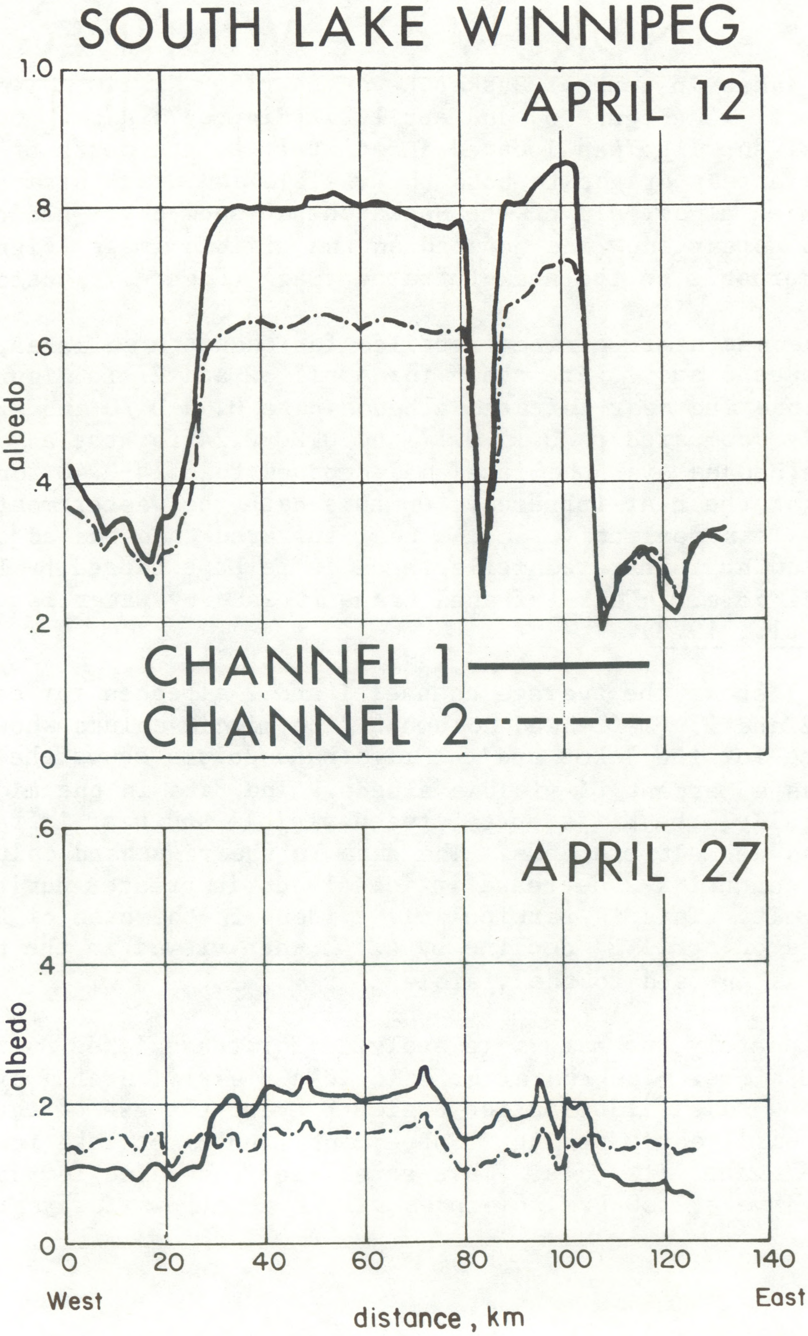

Figure 5 - Albedo trace (B-B on Figures 2 and 3) across southern Lake Winnipeg on April 12, 1980 (top) and April 27, 1980 (bottom).

to the lake is roughly equivalent to that of the snow/ice on the lake itself, virtually masking the southern part of Lake Winnipeg on the satellite image (the lower image in Figure 3). This is consistent with information on reflectance of vegetation and chlorophyll given by Hoffer and Johannsen (1969).

Three lakes in central Saskatchewan near 55° N, 110° W were also analyzed with the April 12 (Figure 6) and April 27 (Figure 7) data. On April 12, when the regional snowline was located immediately to the north of the lakes, all three lakes appear bright in both the visible and near-infrared images. By April 27, when almost all of the Saskatchewan snow cover had disappeared, the lakes still appear snow/ice covered on the visible image (Figure 7, top), but barely discernable on the near-infrared image (Figure 7, bottom).

Visible and near-infrared profiles for these three lakes, along the line C-C in Figures 6 and 7, are shown for April 12 and 27 in Figure 8. On April 12 the visible and near-infrared albedoes are 0.64-0.70 and 0.51-0.58 respectively, compared to 0.15-0.17 and 0.20-0.24 for the adjacent land. By April 27, albedoes over the lakes had dropped to 0.24-0.40 for the visible and 0.19-0.29 for the near-infrared. On this date the westernmost lake, Egg Lake, is actually less reflective in the near-infrared than the adjoining land. This very low near-infrared reflectance is perhaps caused by liquid water on the snow/ice cover. Near-infrared transmittance by water is very small (Specht et al., 1973).

Table 1 shows the average channel 1 and 2 albedoes for each of the lakes on April 12 and 27 (left-hand column). The middle column shows the channel 1-2 difference for the lakes and the righthand column shows the same difference expressed as a percent of visible albedo. The data in the middle column show that, generally, the difference between visible and near-infrared albedoes becomes less as melt proceeds. The data in the righthand column show that the percentage channel 1-2 decrease in ice albedo is greater during the later stages of melt. This is particularly evident in the case of Egg Lake where ice albedoes on April 27 decline by 42.4% when viewed in the near infrared wavelength as opposed to the visible.

Unfortunately, no data were analyzed for these lakes during frozen mid-winter conditions. The characteristic NOAA-6 early morning overpass, and attendant low solar illumination angles prevent the use of channel 1 and 2 AVHRR data until early spring. Subsequent studies of lake ice will be done using NOAA-7 satellite data. This satellite, scheduled for launch in July 1981, will have a 2:30 P.M. overpass time that allows for year-round snow and ice studies.

Snowcover

Satellite data have been used in observations of mountain and prairie snowcover since the early 1960's (Barnes and Smallwood, 1975). A recently completed NASA-sponsored Applications Systems Verification Test (ASVT) demonstrated the cost-effectiveness of including satellite snowcover data in the management of water resources in the western United States (Rango,

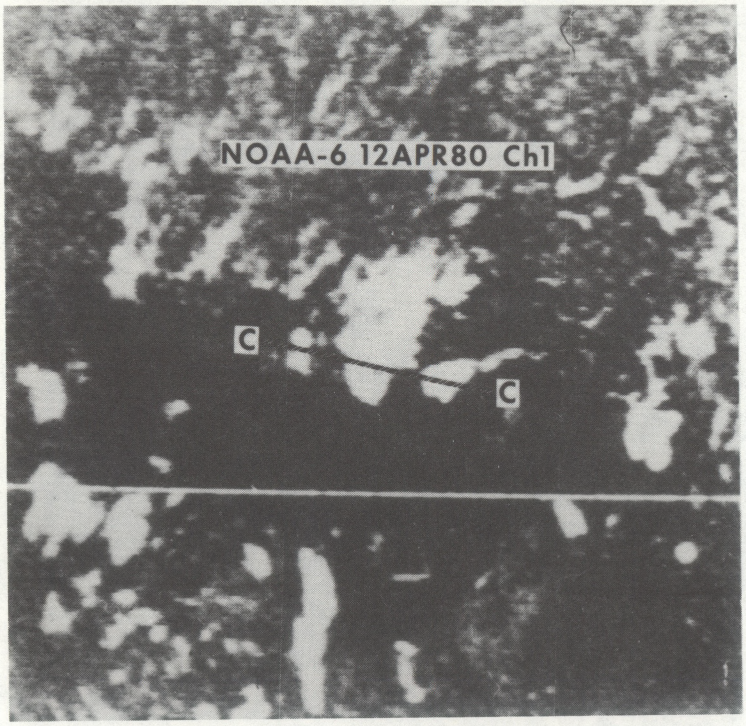

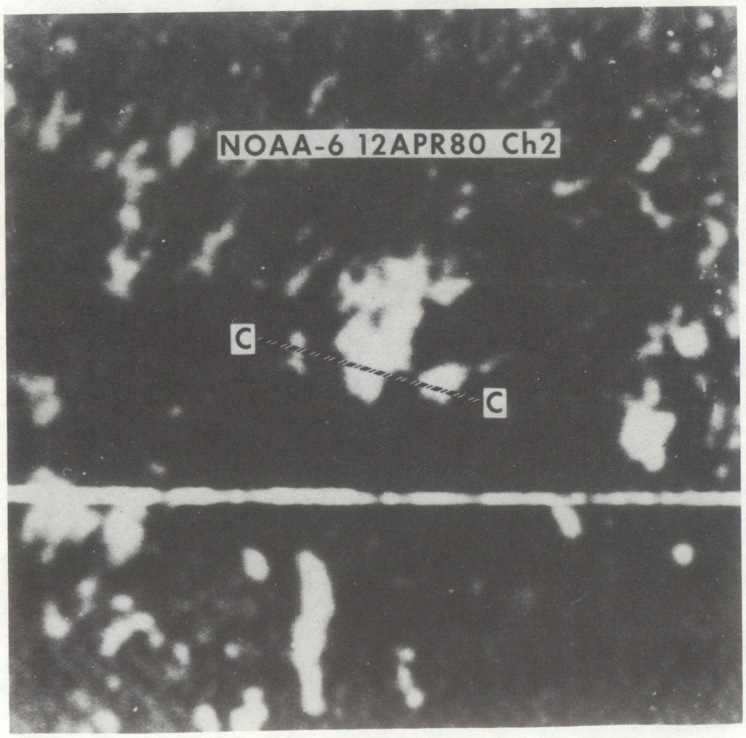

Figure 6 - Visible (top) and near-infrared (bottom) images of Egg Lake, Lac La Ronge, and Wapawekka Lake, on April 12 at 7:59 a.m. local time.

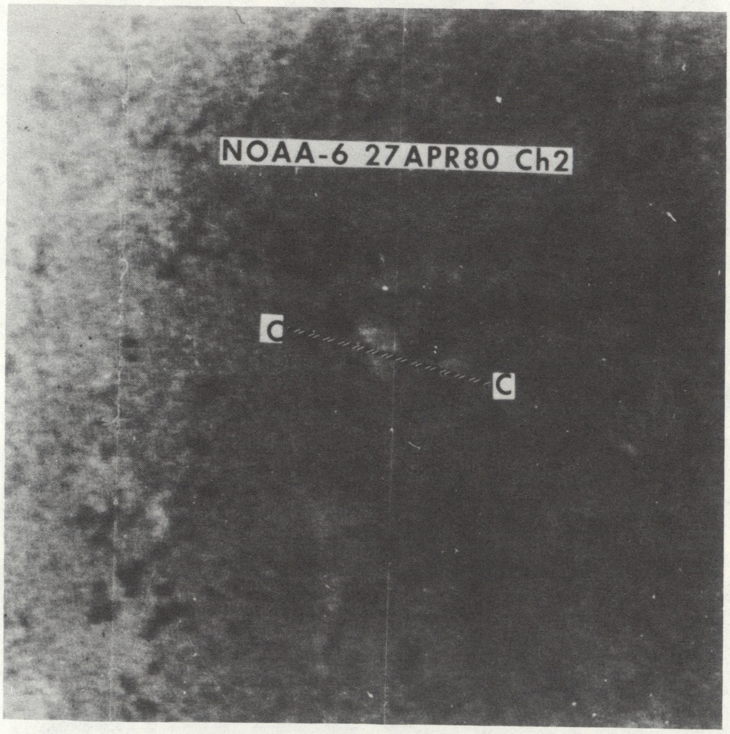

Figure 7 - Visible (top) and near-infrared (bottom) images of Egg Lake, Lac La Ronge, and Wapawekka Lake on April 27.

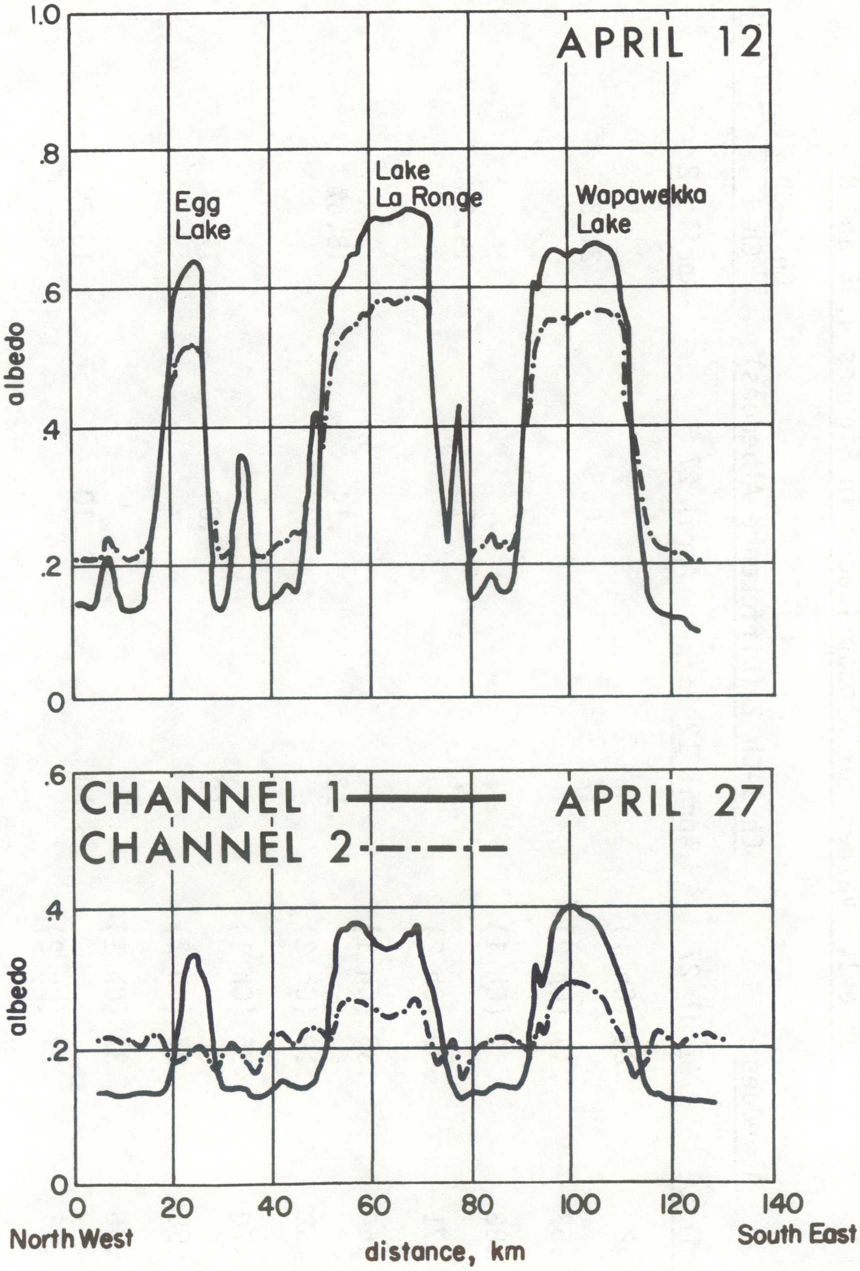

Figure 8 - Albedo trace (C-C on Figures 6 and 7) on April (top) and April 27 (bottom)

Table 1. Values for Albedo Traces in Figures 4, 5 and 8

	Albedoes		Ch 1-Ch 2 (Difference Albedoes)		$\frac{\text{Ch 1-Ch 2}}{\text{Ch 1}}$ x100 (Percentage Albedo Decrease)	
	April 12	April 27	April 12	April 27	April 12	April 27
S. Winnepeg	.8	.23 (Ch 1)	.17	.06	21.3%	26.1%
	.63	.17 (Ch 2)				
N. Winnepeg	.88	.52 (Ch 1)	.17	.13	19.3%	25.0%
	.71	.39 (Ch 2)				
Egg Lake	.64	.33 (Ch 1)	.12	.14	18.8%	42.4%
	.52	.19 (Ch 2)				
Lac La Ronge	.70	.36 (Ch 1)	.12	.09	17.1%	25.0%
	.58	.27 (Ch 2)				
Wapawekka	.66	.37 (Ch 1)	.10	.10	15.2%	27.0%
	.56	.27 (Ch 2)				

1980). An operational snowmapping program was inaugurated at NOAA in 1974 and now serves more than 30 selected watersheds in the western United States (Schneider,1980). Although visible data have proved to be superior for definition of snow extent, the near-infrared holds the promise of providing additional useful information on the condition of the snowpack. Figure 9 contains response curves for a non-melting and melting snow surface as determined experimentally at the Army Cold Regions Research and Engineering Laboratory (O'Brien and Munis, 1975). The experiments were conducted on snow samples of 10 cm depth. As can be seen, snow has a very high reflectance in the visible region of the spectrum and falls off sharply in the near-infrared. Snow reflectivity decreases rapidly throughout most of the near infrared portion of the spectrum with the onset of surface melt. Attempts to reproduce the O'Brien and Munis findings with satellite data have met with only partial success owing to sensor limitations and substrate influence on snowcover response.

Eschner et al (1977) showed that, in contrast to the findings of O'Brien and Munis, snowcover reflectivity in the Adirondack Mountains actually increased in the near infrared (Landsat Band 7). The increase in snow reflectance was no doubt caused by the effect of the dense foliage ie; coniferous and deciduous forests.

Wiesnet et al (1974) found that a disturbing feature of monitoring snowcover from digitized Landsat MSS data was the low threshold of saturation, particularly in band 5. During the early melt season in the Sierra Nevada Mts, more than 75 percent of the snow pixels had brightness value at saturation. In band 7, 25 percent of the pixels reached saturation. The designed upper limits of 36 percent albedo in band 5 and 48 percent in band 7 (Dozier, 1981) are much too low for multispectral studies of bright snow surfaces. Landsat was, of course, designed for earth resource surveys and not for snow studies. Mention was made (General Electric Corp, 1972) that clouds may often saturate the MSS; unfortunately, snow has similarly high brightness values. NOAA-6, on the other hand, is designed to permit studies of highly reflective targets; ie clouds, ice and snow. Consequently the saturation levels in AVHRR channels 1 and 2 are set respectively at 79.1 percent and 93.1 percent albedo (ITT, 1980).

For this report, five different transects (Figure 10) were selected from the previously mentioned April 12th NOAA-6 pass (orbit 4123). Three of the study areas were located in mountainous regions of Wyoming and Colorado; the remaining area, having two transects, lies in the prairie region of western Kansas and Nebraska. Figure 11 contains channel 1 and 2 profiles taken along a 160 km NW-SE transect in the Wyoming-Colorado border area. This line is labelled D-D on Figure 10. Albedoes of deep prairie snow as well as snow above the timberline peak at about .70 in channel 1 and .62 in channel 2. Note that due to the masking effect of foliage, snowcovered forest actually exhibits higher albedoes in channel 2 than channel 1. This channel 2-channel 1 difference varies directly with the density of forest canopy. The densest (darkest) snowcovered forests on the profile have channel 2-channel 1 differences of .10 while snowcover in sparse woodland is almost equally reflective in both channels.

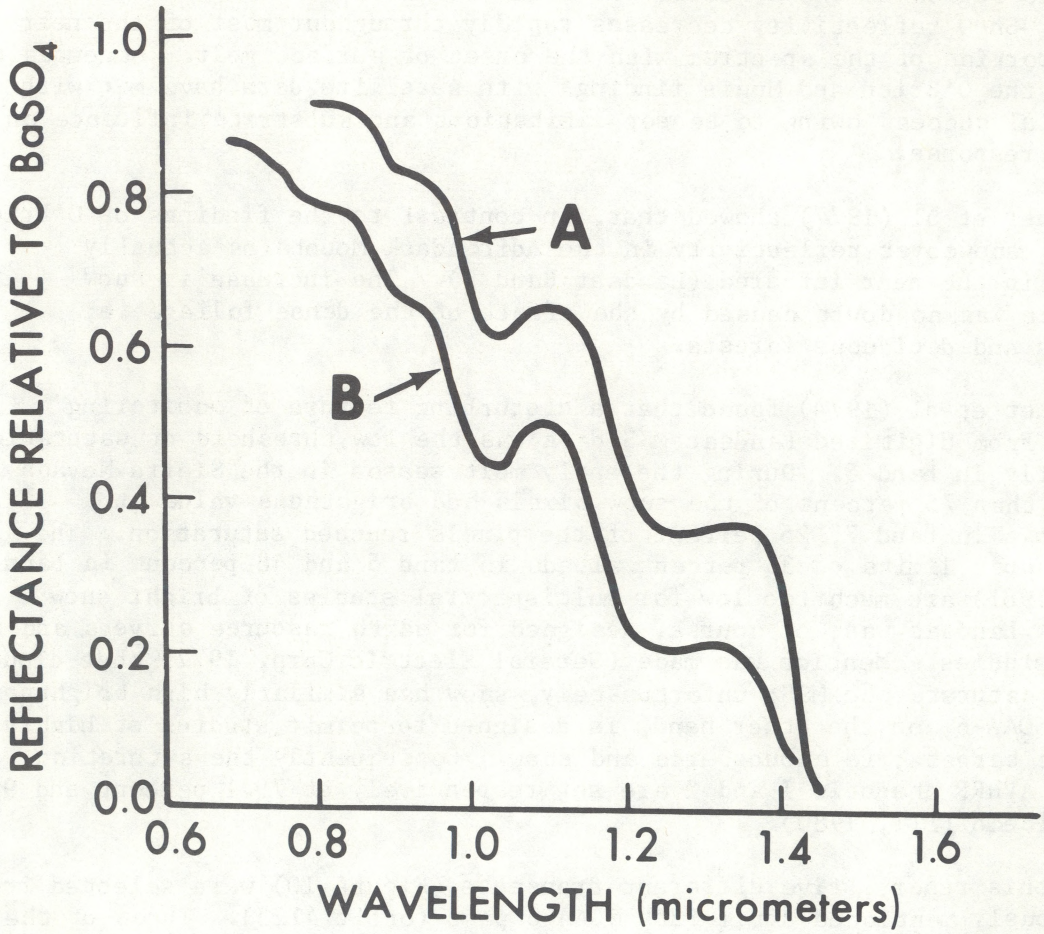

Figure 9 - Spectral response curves for a nonmelting (A) and melting (B) snow surface (after O'Brien and Munis, 1975)

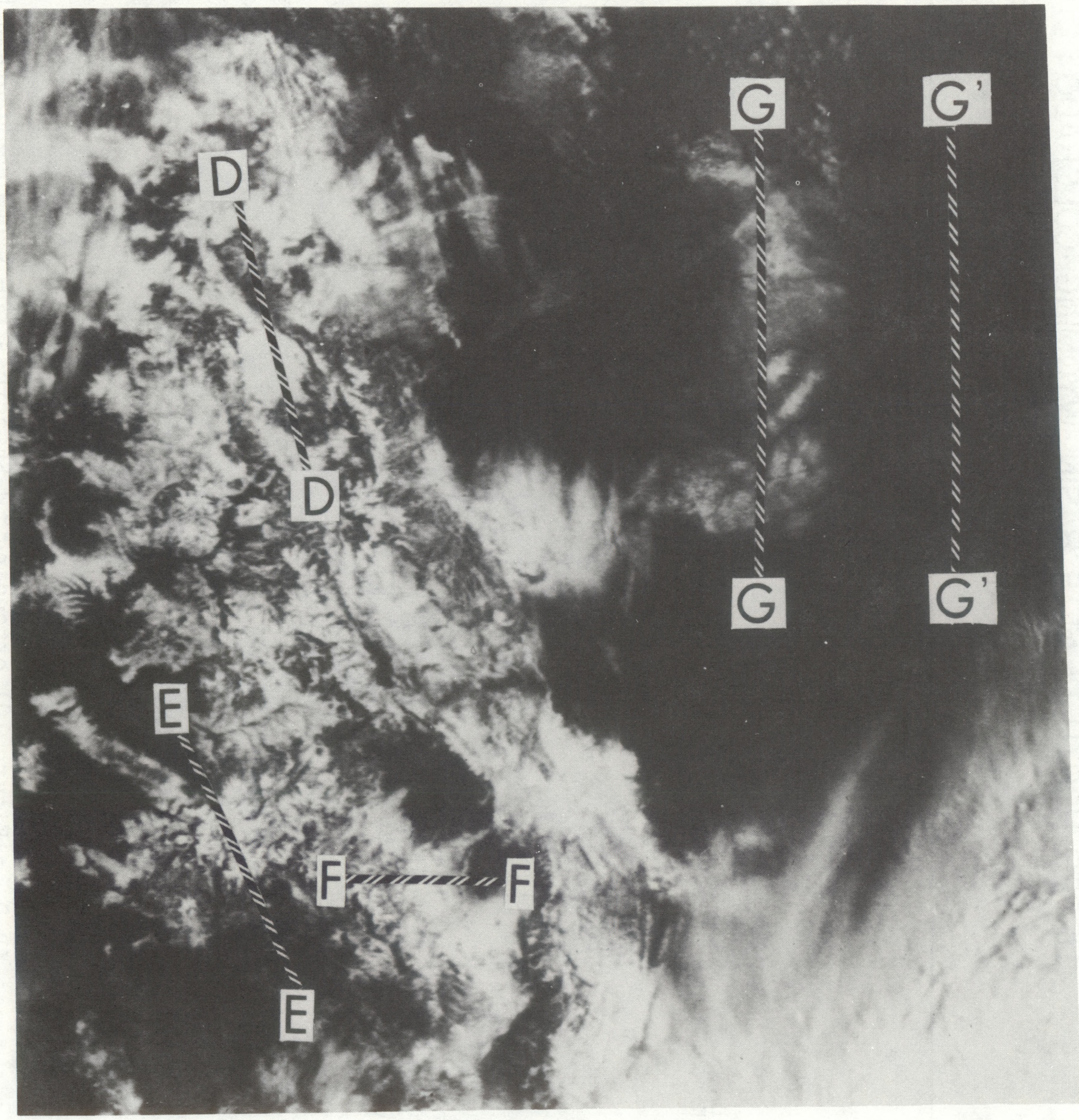

Figure 10 - Blow-up of a portion of the April 12th NOAA-6 image, orbit #4123, showing the partially snowcovered Rocky Mountains and Great Plains.

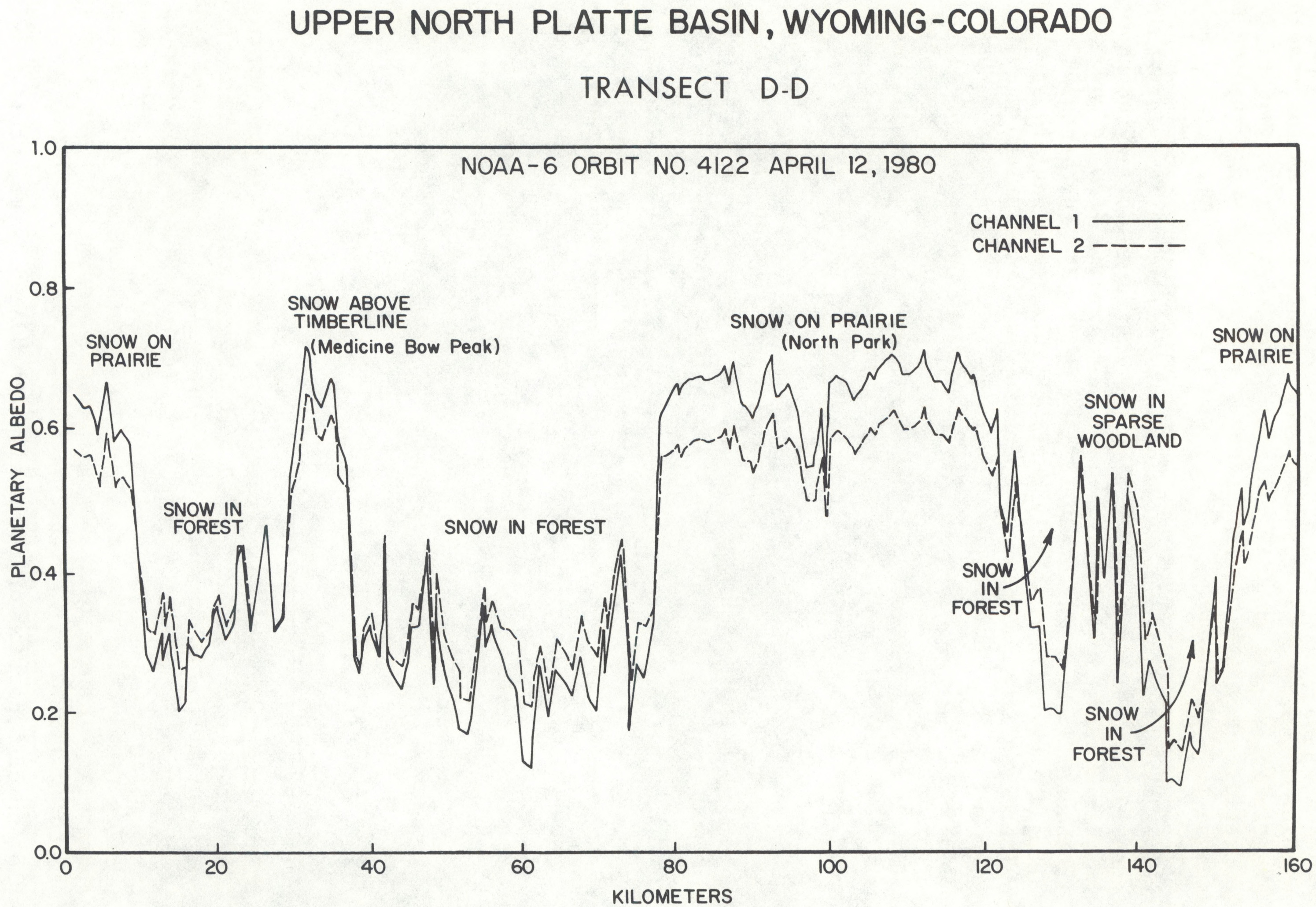

Figure 11 - Albedo trace (D-D on Figure 10) extending NW-SE across the Wyoming-Colorado border.

Another 160 km NW-SE profile was studied in the San Juan Mt. region of western Colorado. This transect is labelled E-E on Figure 10. On the profile (Figure 12) the heightened response of vegetation and foliage in the near-infrared is indicated by increased channel 2 reflectances for snowfree prairie as well as within both snowfree and snowcovered forest. Only in the case of snow above the timberline did channel 1 albedoes exceed those of channel 2. Identical low reflectances are found in steep river valleys where shadows mask the snow response in both channels.

A 110 km W-E profile for the upper Rio Grande watershed in Colorado is shown in Figure 13; the transect is labelled F-F on Figure 10. As on the other profiles, snow above the timberline and deep prairie snow is more reflective in channel 1; snow in forest is more reflective in channel 2. Elevations along this profile generally decrease going from west to east; a sharp change in terrain from mountain to prairie (San Luis Valley) occurs at about the 40 km mark. The prairie snow decreases in depth until the snowline is reached at about the 90 km mark. As the snow depth decreases underlying grass and shrubs begin to account for more and more of the albedo response causing the channel 1 and 2 curves to draw together. At a point near the snowline, the channel 1 and 2 reflectivities interchange with those of channel 2 becoming characteristically dominant on the snowfree prairie.

The channel 1 and 2 profiles in Figure 14 were determined over a 280 km N-S transect in western Nebraska and Kansas (labelled G-G on Figure 10). Snowcover on this date ranged from trace amounts to about 10 cm (4 in) (NOAA, 1980). For a shallow snow pack such as this, it can be assumed that snow brightness varies directly with depth (McGinnis, 1975). On this profile, the greatest channel 1 -channel 2 differences occur over the brightest (deepest) snowcover. It can again be seen that as snow depths decrease, the underlying vegetation causes the channel 1 and 2 response to merge. The channel 2 curve does not cross channel 1 until the snowline is reached at the 250 km mark.

Figure 15 shows another 280 km profile in Kansas and Nebraska (G'-G' on Figure 10) which runs in a north-south direction at a distance approximately 150 km parallel and east of line G-G. This profile shows a typical grassland response with channel 2 reflectivities in the .15 range and channel 1 reflectivities averaging about .11. Note the homogeneity of albedoes in this region of Nebraska and Kansas given the absence of snowcover.

Water Penetration/Land-Water Interface

Landsat MSS data have been found useful for lake water quality monitoring by several investigators. Wiesnet (1976) demonstrated the use of Landsat for monitoring sediment inflow to Canada's Great Slave lake. Scarpace and Fisher (1980) classified approximately 5000 Wisconsin lakes into seven different trophic classes using digitized Landsat data. Strong and Eadie (1978) used data from Landsat, NOAA-2 and Skylab to map the occurrence and distribution of calcium carbonate precipitate in the Great Lakes. Sydor (1980) was able to estimate the concentration of particulates in western Lake Superior to within 0.05 mg/liter when comparing data from Landsat and an auxiliary ground-based NASA radiometer.

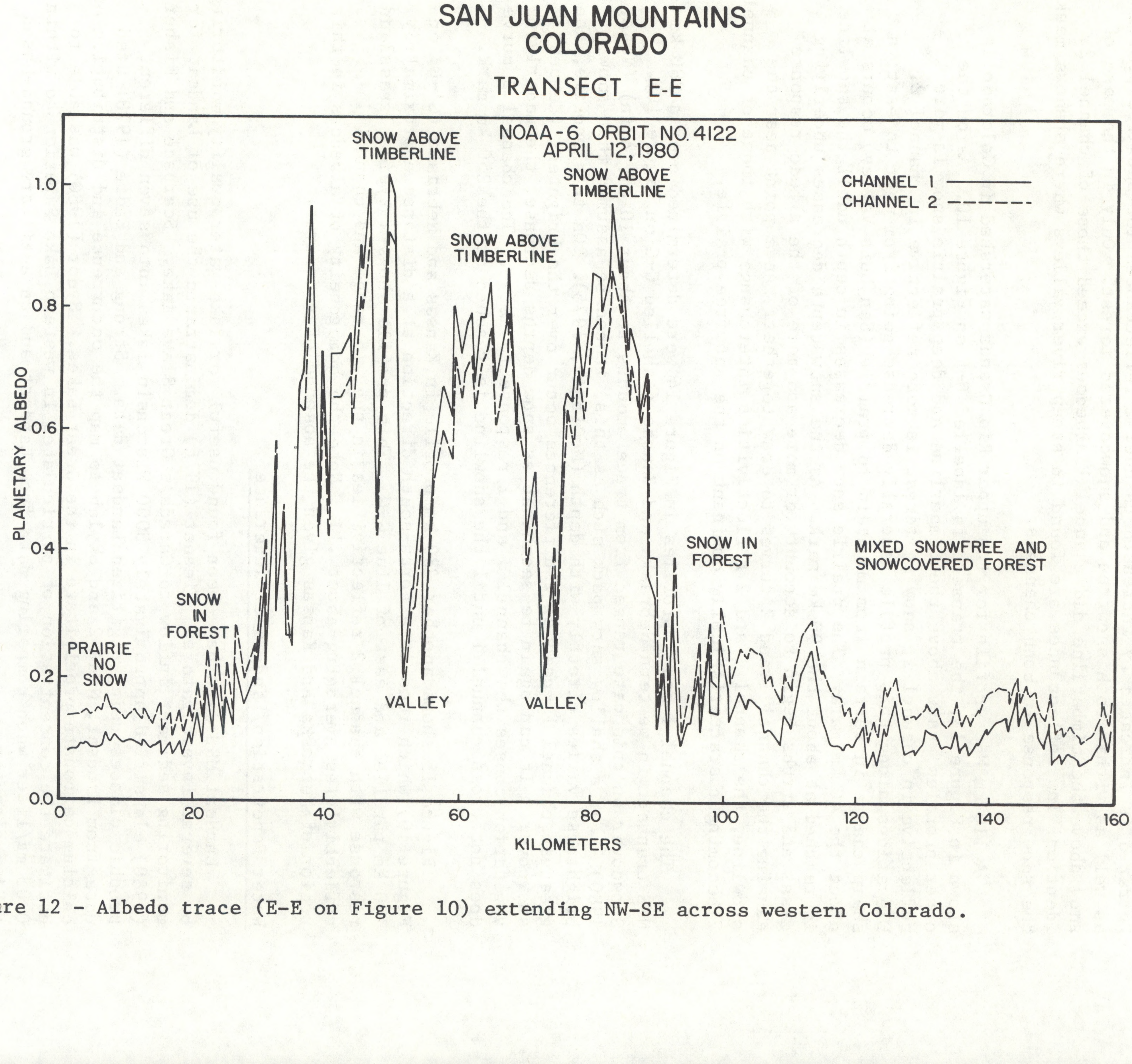

Figure 12 - Albedo trace (E-E on Figure 10) extending NW-SE across western Colorado.

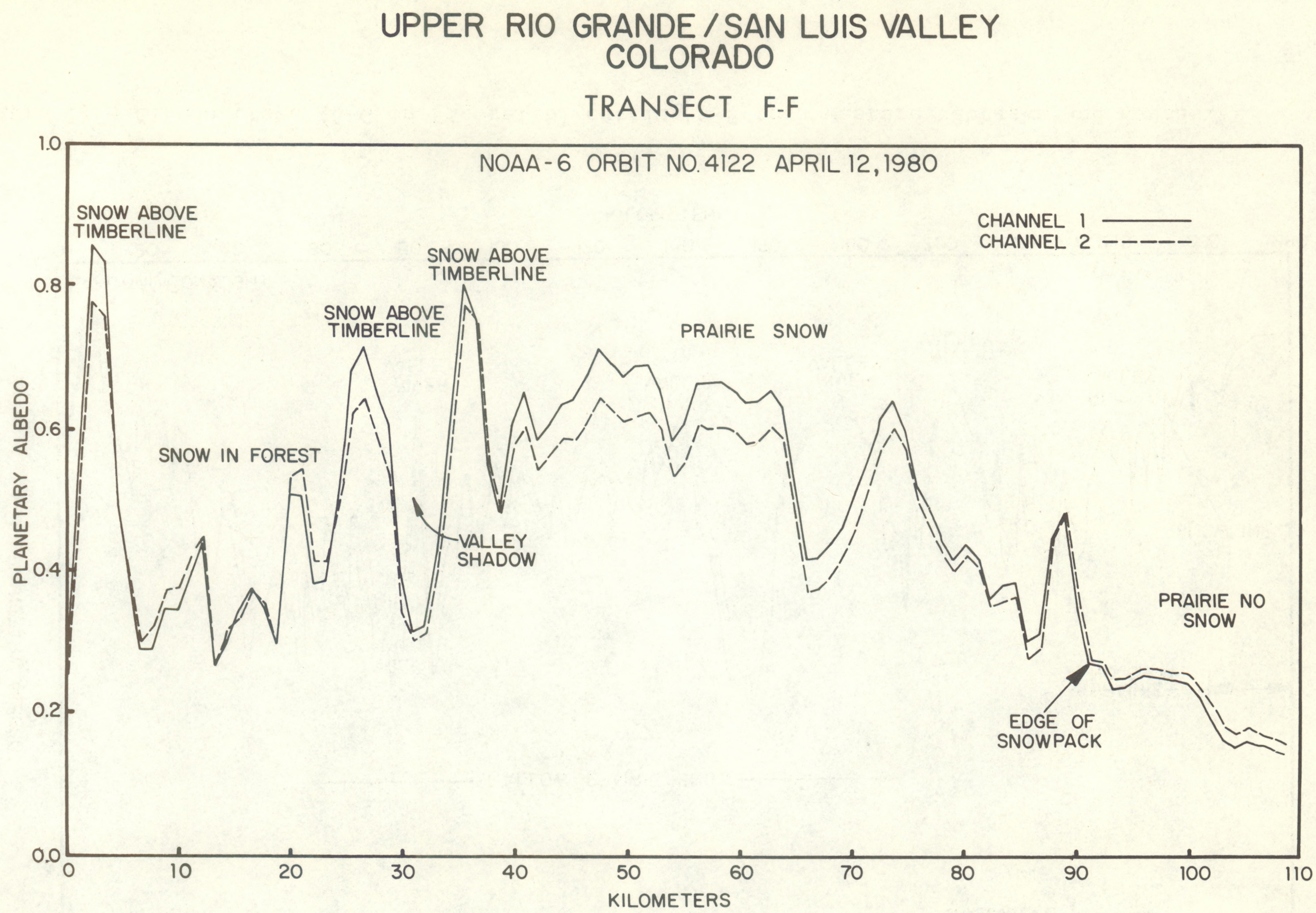

Figure 13 - Albedo trace (F-F on Figure 10) extending W-E across central Colorado.

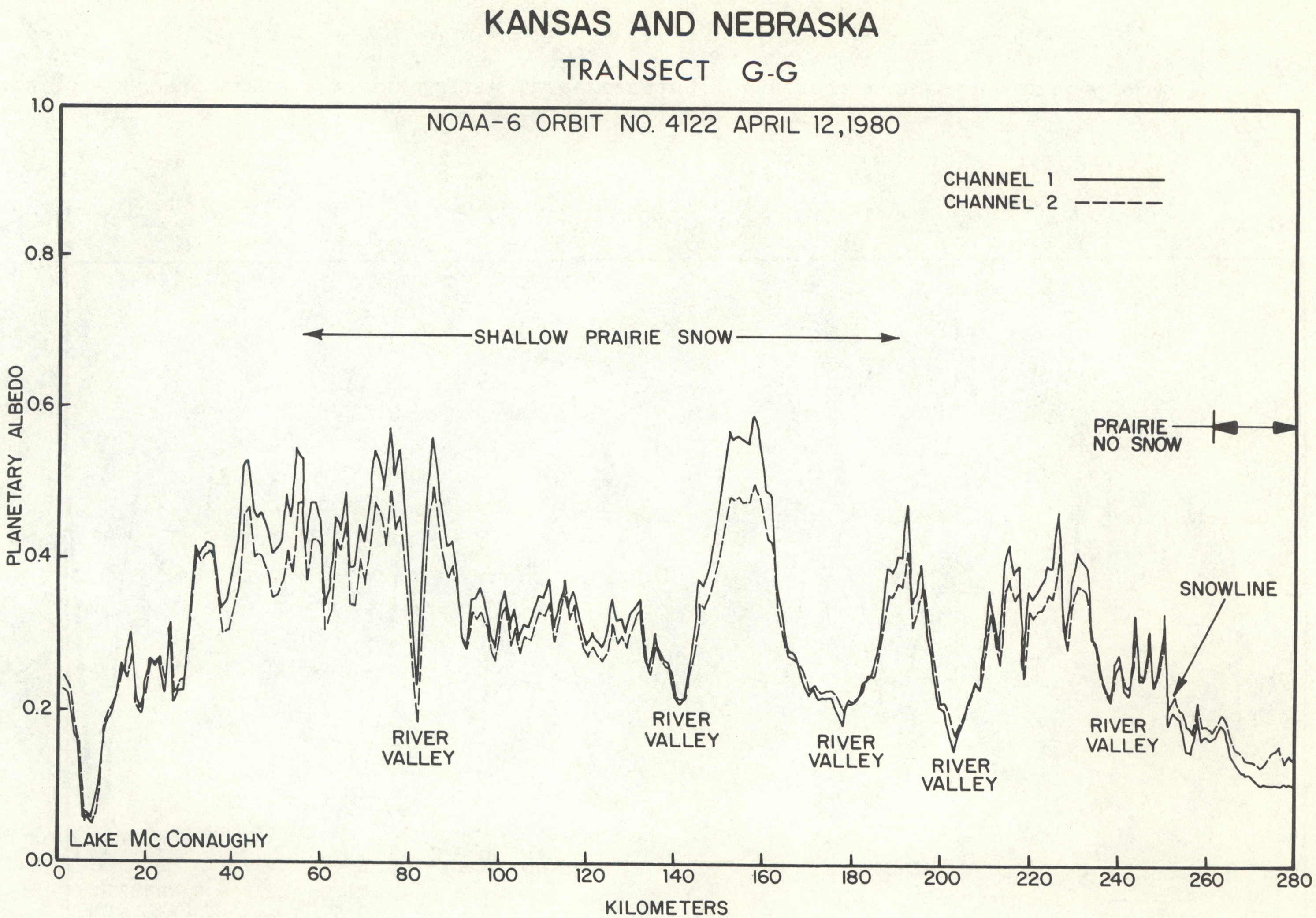

Figure 14 - Albedo trace (G-G on Figure 10) cutting N-S thru western Nebraska and Kansas.

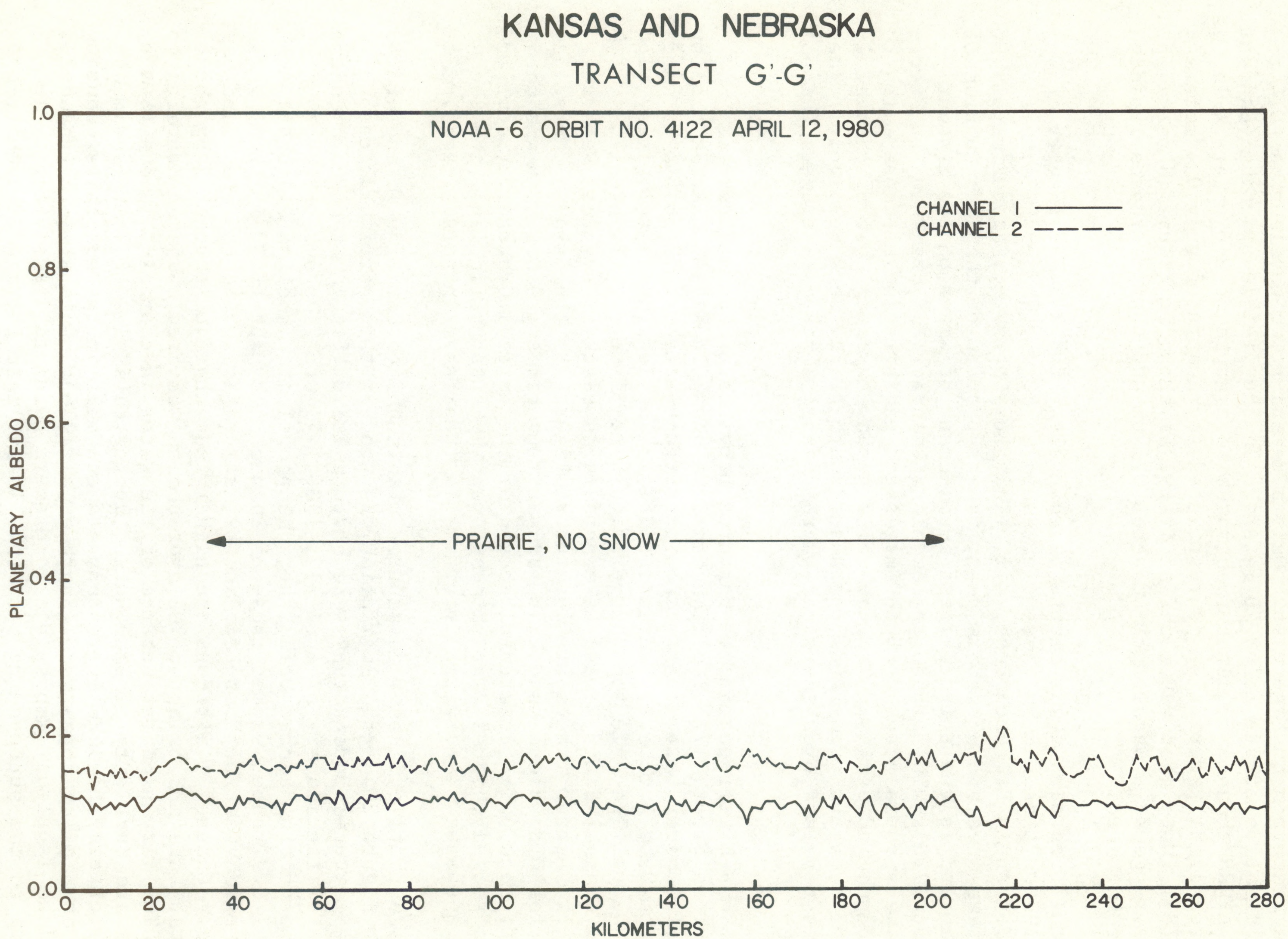

Figure 15 - Albedo trace (G'-G' on Figure 10) cutting N-S thru Central Nebraska and Kansas.

With few exceptions, water quality studies conducted with Landsat have utilized data in the shorter wavelength portion of the spectrum; i.e., MSS bands 4 and 5. The ability of light in various wavelengths to penetrate water is shown in the graph on Figure 16. Only blue and green wavelengths (0.4 to 0.6 um) of light penetrate below 20 meters. In the visible spectrum (Landsat band 5 and AVHRR channel 1) light penetrates to a depth of 3-6 meters. In the near-infrared light penetration is restricted to a depth of only 0.1 meters (Moore, 1978). Note that water reflectivity, as shown in Figure 16 peaks in the visible range at a wavelength of about 0.5 um and then decreases rapidly in the near-infrared.

Figure 17 contains enlargements of channels 1 and 2 AVHRR imagery of April 27, 1980. Line H-H on these figures is an 80 km, N-S profile that transects Montana's Ft. Peck Reservoir. This body of water, approximately 980 km^2 in surface area and 67 meters deep, is a byproduct of the construction of Ft. Peck Dam and is the third largest impoundment of water on the Missouri River (Todd, 1970). The albedo traces along transect H-H are shown in Figure 18. The lake appears black on both images and exhibits low albedoes owing to its great depth and purity. The channel 2 reponse exceeds that of channel 1 by about .03 over the grasslands north and south of Ft. Peck Reservoir. The situation is reversed over the water where channel 1 response exceeds that of channel 2 by .01.

A 160 km W-E transect in the Canadian province of Saskatchewan is labelled I-I on Figure 17. The transect cuts thru Old Wives' Lake, a shallow intermittent body of water that varies in surface area from 0 to 395 km^2 and in depth from 0 to 3 meters (Pentland, 1981). The lake has a relatively high albedo in channel 1 and is somewhat difficult to discern on Figure 17. However, in channel 2 Old Wives' Lake appears as black as Ft. Peck Reservoir to the south. Albedo traces are located at Figure 19; they show a channel 1-2 difference for Old Wives' Lake that is over four times greater than was the case for Ft. Peck. The lowered albedoes for the water in channel 2, combined with the increased channel 2 brightness over the surrounding land, are the reason for a sharper land-water interface in these near-infrared images.

Two more profile lines were studied within the border of Utah and are depicted in Figure 20. An illustration was used in this particular case because the features under study were obscure and difficult to discern on the original satellite imagery of April 12, 1980. Figure 21 shows a 50 km W-E profile line cutting across Utah lake; the profile is labelled J-J on Figure 20. Channel 2 albedoes exceed those of channel 1 by about .03 in the vegetated region west of Utah Lake and by as much as .09 in the crop land east of the lake. Channel 1 albedoes are higher than those of channel 2 by about .09 over Utah Lake and by about .02 over the snowcovered, Wasatch Moutains to the east. The very high reflectance of the water in channel 1 is due to the shallowness and turbidity of Utah Lake. During this time of year, sediment-laden water enters the lake in response to snowmelt in the mountains, causing it to take on a milky appearance (Short et al 1976). On a visible (channel 1) image the lake is almost impossible to discern owing to its similarity in reflectivity to the surrounding terrain. In the near infrared, however, the lake stands out clearly due to a combination of lower water albedoes and brighter land response.

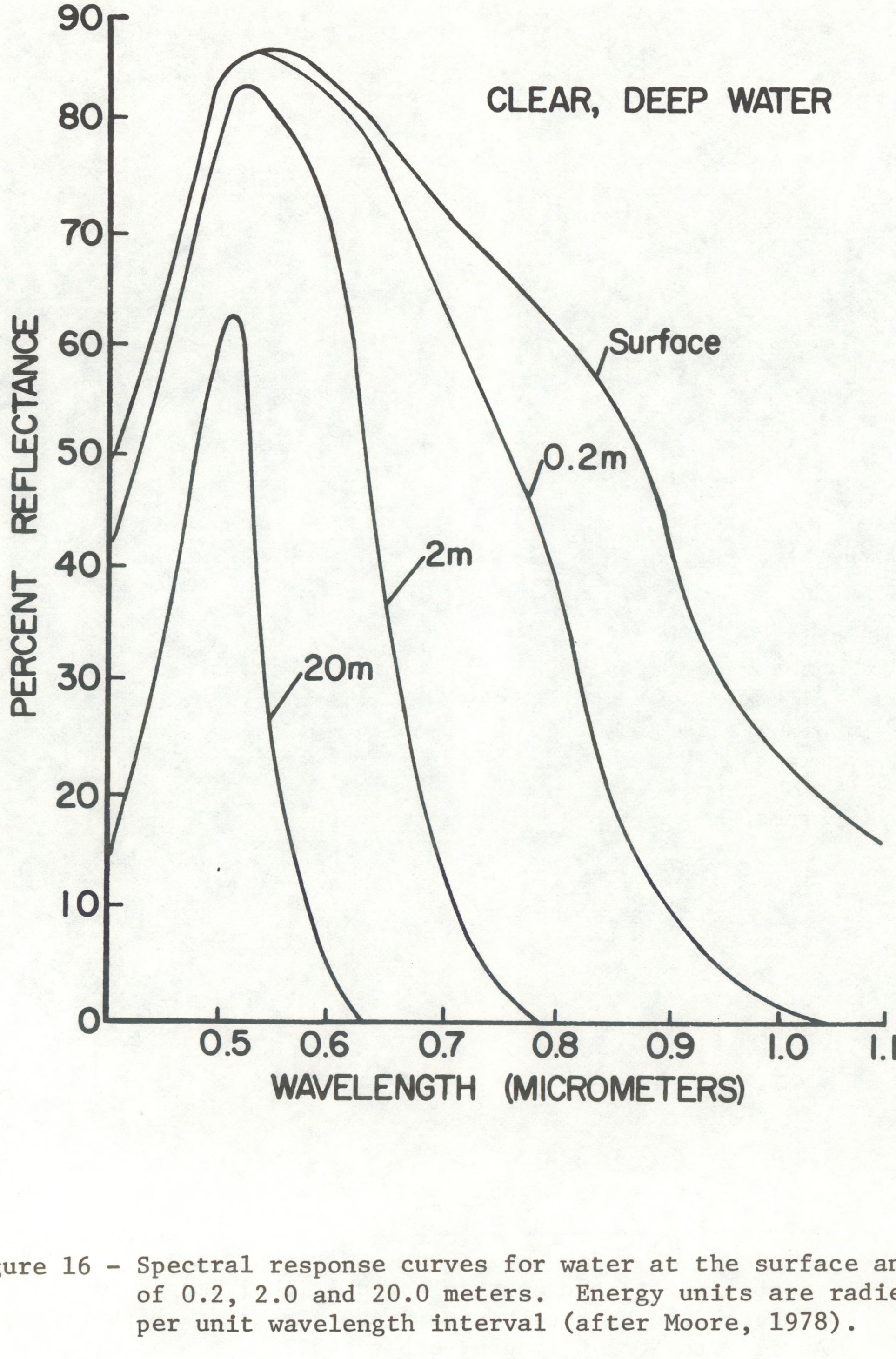

Figure 16 - Spectral response curves for water at the surface and depths of 0.2, 2.0 and 20.0 meters. Energy units are radient flux per unit wavelength interval (after Moore, 1978).

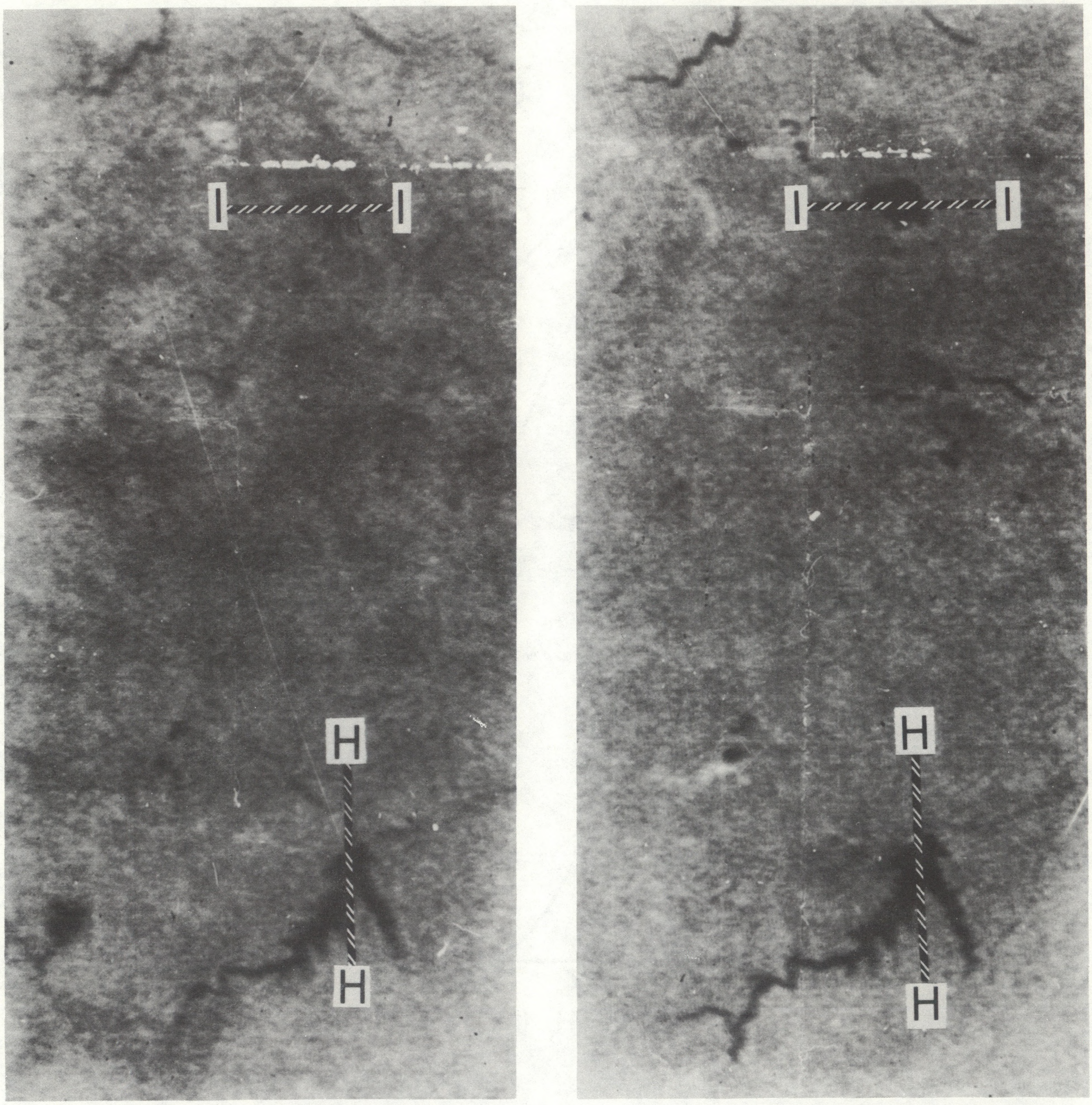

Figure 17 -- Visible (left) and near-infrared (right) images of the Saskatchewan-Montana border area. These are blow-up of the April 27th NOAA-6 images, orbit #4322.

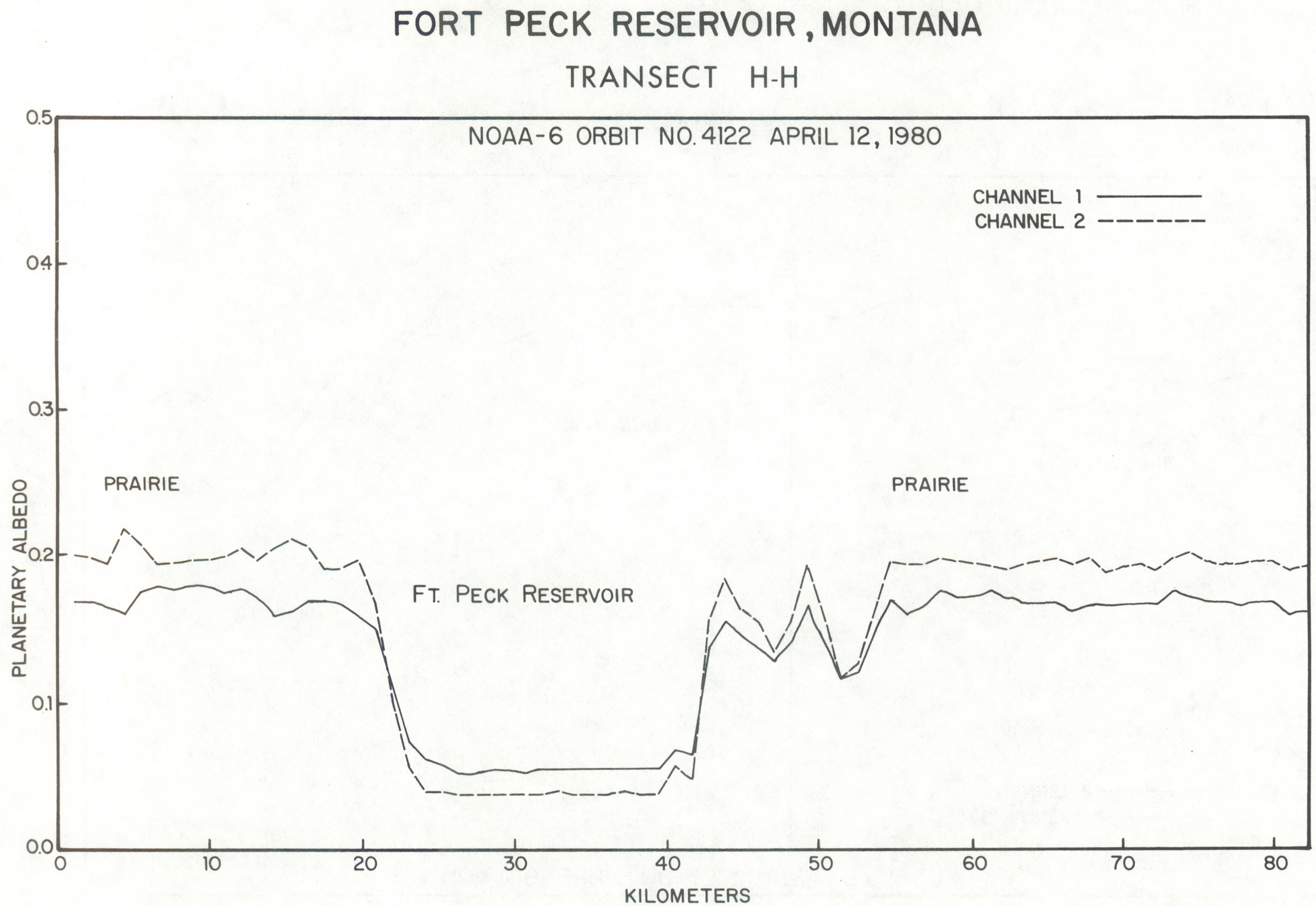

Figure 18 - Albedo trace (H-H on Figure 17) cutting N-S thru Ft. Peck Reservoir in Central Montana.

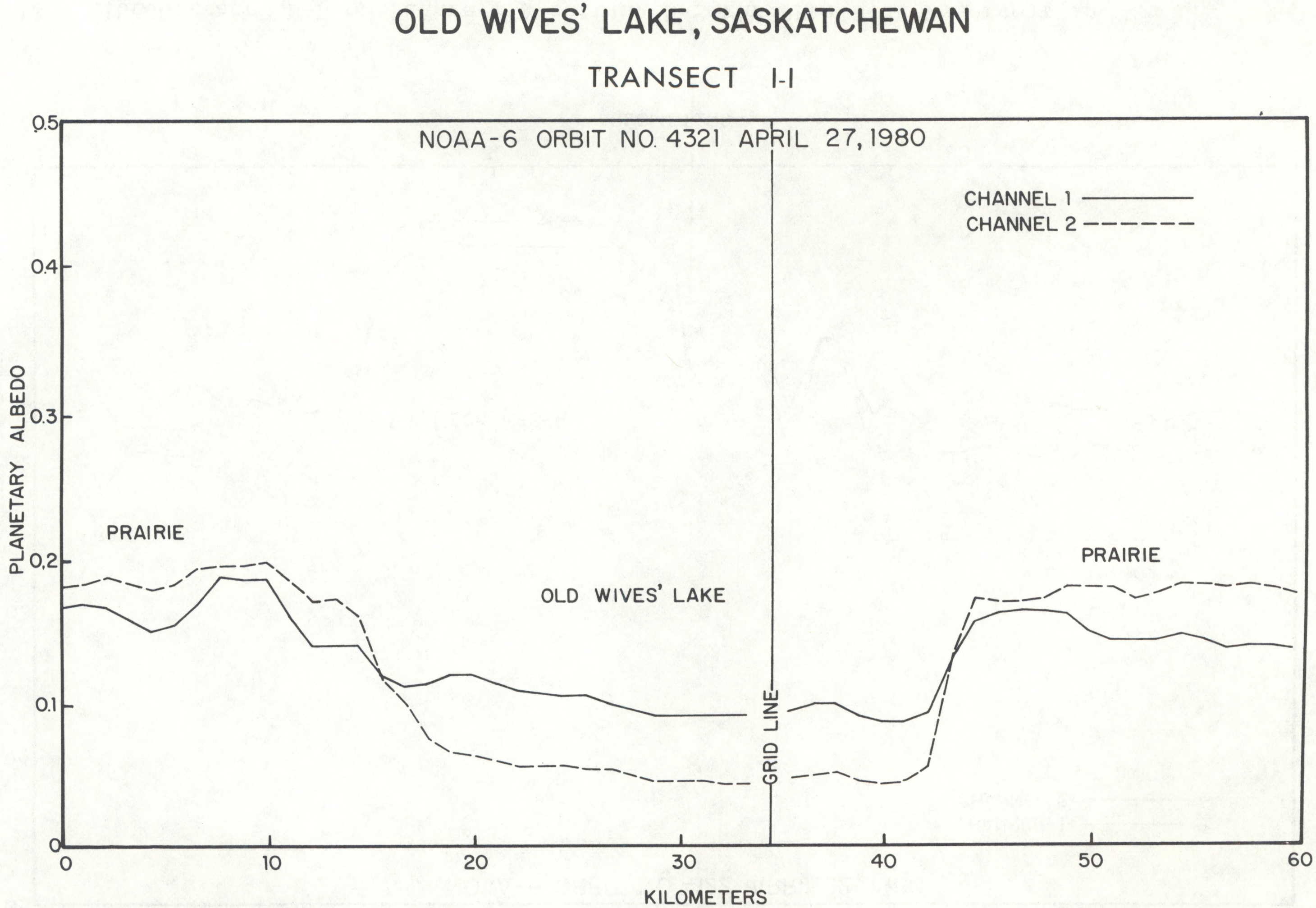

Figure 19 - Albedo trace (I-I on Figure 17) extending W-E across Old Wives' Lake and the southern Saskatchewan region. The grid line was imbedded on the digital data for earth location purposes.

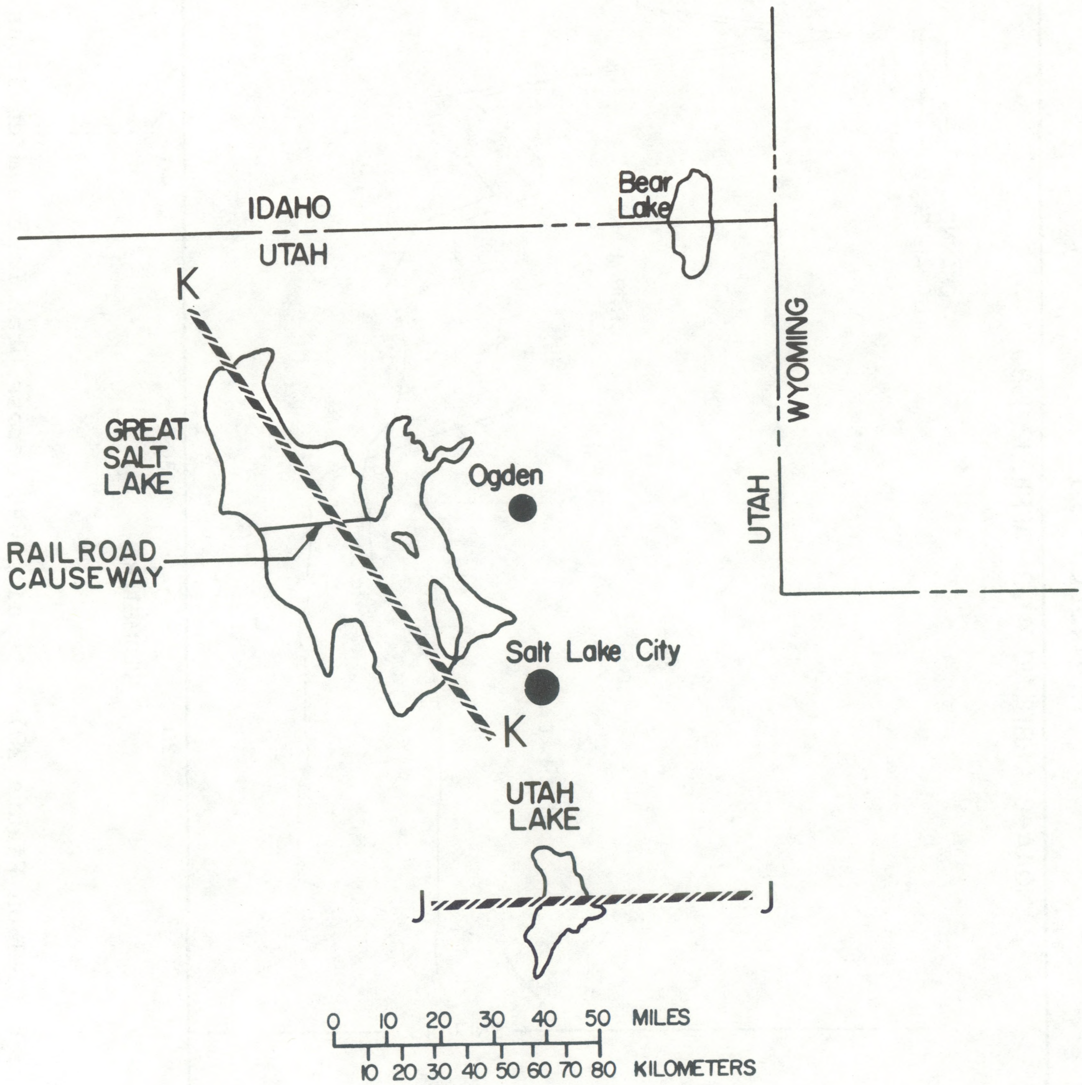

Figure 20 - Illustration showing Utah Lake, Great Salt Lake and environs. Note the railroad causeway nearly bisecting Great Salt Lake.

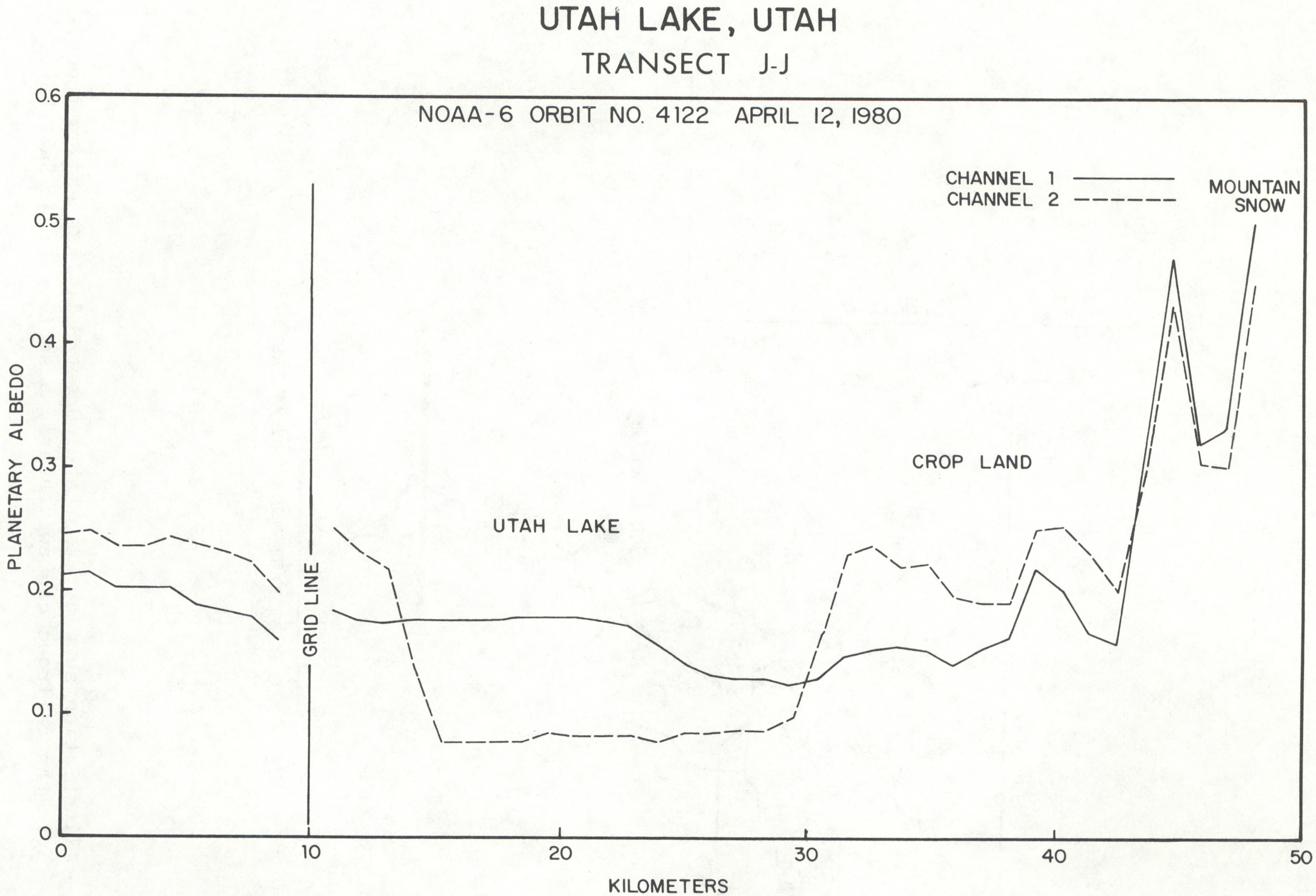

Figure 21 - Albedo trace (J-J on Figure 20) extending W-E across Utah Lake and environs. The grid line was imbedded on the digital data for earth location purposes.

Transect K-K in Figure 20 extends 140 km NW-SE cutting diagonally across Great Salt Lake; albedo traces along this line are shown in Figure 22. Great Salt Lake has a surface area of over 2500 km^2 but a maximum depth of only 9 meters. The lake is essentially divided into two basins, the north and south arms, by a semipermeable rockfill railroad causeway constructed during the two year period 1957-1959 (Matson and Berg, 1981). Owing to the interruption of circulation by the causeway of the Southern Pacific railroad, the lake has become more saline in the north and exhibits a uniformly turbid appearance best seen in shorter wavelengths; i.e., Landsat band 4 and 5 (Short el al 1976). Since more than 90 percent of the fresh water inflow enters the south arm (Lin et al, 1972), the north arm is little more than an evaporation basin. The difference in reflectivity between north and south arm can be seen in Figure 22. North of the causeway channel 1 albedoes are a uniform 0.13; south of the causeway channel 1 albedoes drop to less than 0.06. Channel 2 albedoes on the other hand are almost constant on either side of the causeway. On visible satellite images the disparity between the north and south arms is readily apparent to the naked eye; on near infrared images the lake appears uniformly black.

Data for the four lakes studied in this section (profiles H-H through K-K) are presented in Table 2. The table shows that shallow, turbid lakes ie; Old Wive's, Utah and Great Salt north arm, have the greatest channel 1 albedoes and large channel 1-2 differences. A clear deep lake such as Ft. Peck, will have a low visible (channel 1) albedo and small channel 1-2 difference.

Vegetation Monitoring/Terrain Classification

The usefulness of visible and near-infrared wavelengths of light in terrain and crop classification, determination of acreage under cultivation and the monitoring of crop condition is well documented in the literature. Tucker et al. (1980) found that visible and near-infrared data from hand-held radiometers could be used to indicate vigor and condition of plant canopy. Holben et al. (1980) used similar data to accurately measure green leaf area and green leaf biomass. Tucker et al. (1980) successfully related combinations of visible and near-infrared data to subsequent grain yield. Thompson and Wehmanen (1980) used Landsat digital data to detect moisture stress in corn and soybean growing regions. Leaf area index estimates for wheat from Landsat were reported on by Wiegand et al (1979).

The response of a green leaf (chlorophyll) in various wavelengths of light is shown in Figure 23. Note that green leaf reflectance dips low in the visible wavelengths and bottoms out near .65 um. Response increases exponentially in the near-infrared portion of the spectrum (i.e., Landsat MSS band 7 and AVHRR channel 2).

The increased terrain response in AVHRR channel 2 when compared to channel 1 has already been demonstrated for prairie grasslands (Figure 15). The high chlorophyll density associated with alpine forests was actually found to mask and indeed, reverse the "normal" drop in channel 2 snowcover reflectance (Figures 11, 12, and 13). As expected, the greatest channel 2

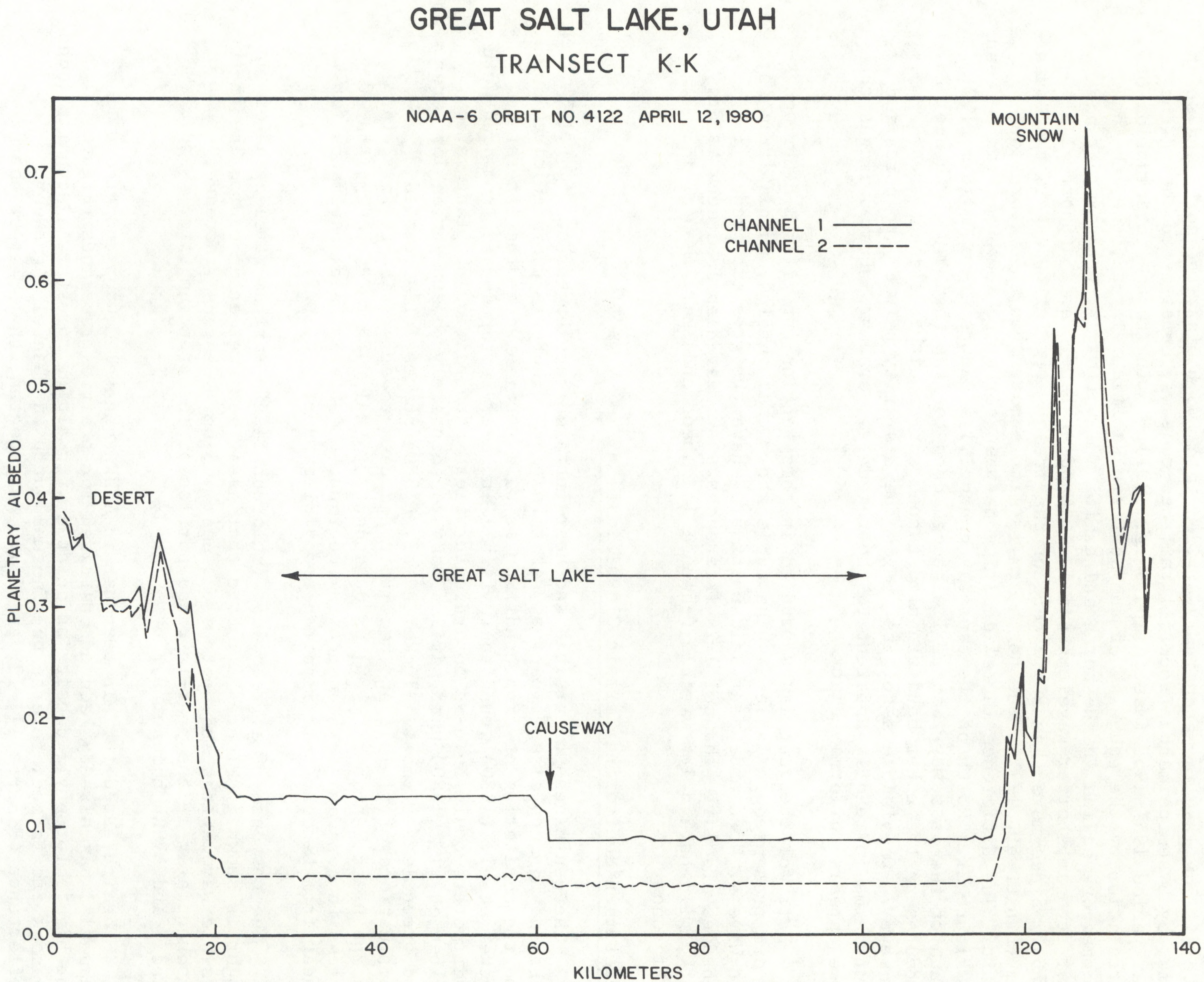

Figure 22 - Albedo trace (K-K on Figure 20) cutting NW-SE across Great Salt Lake.

Table 2. Albedoes for Selected Lakes

	Surface Area (km^2)	Max. Depth (m)	Ch 1 Albedo	Ch 2 Albedo	Ch 1-2
Ft. Peck	980.0	67.1	.055	.045	.01
Old Wives' Lake	395.4	3.0	.10	.055	.045
Utah	378.9	6.1	.18	.09	.09
Salt Lake	2560.0	9.2	.13 (north arm) .09 (south arm)	.055 (north arm) .050 (south arm)	.075 .040

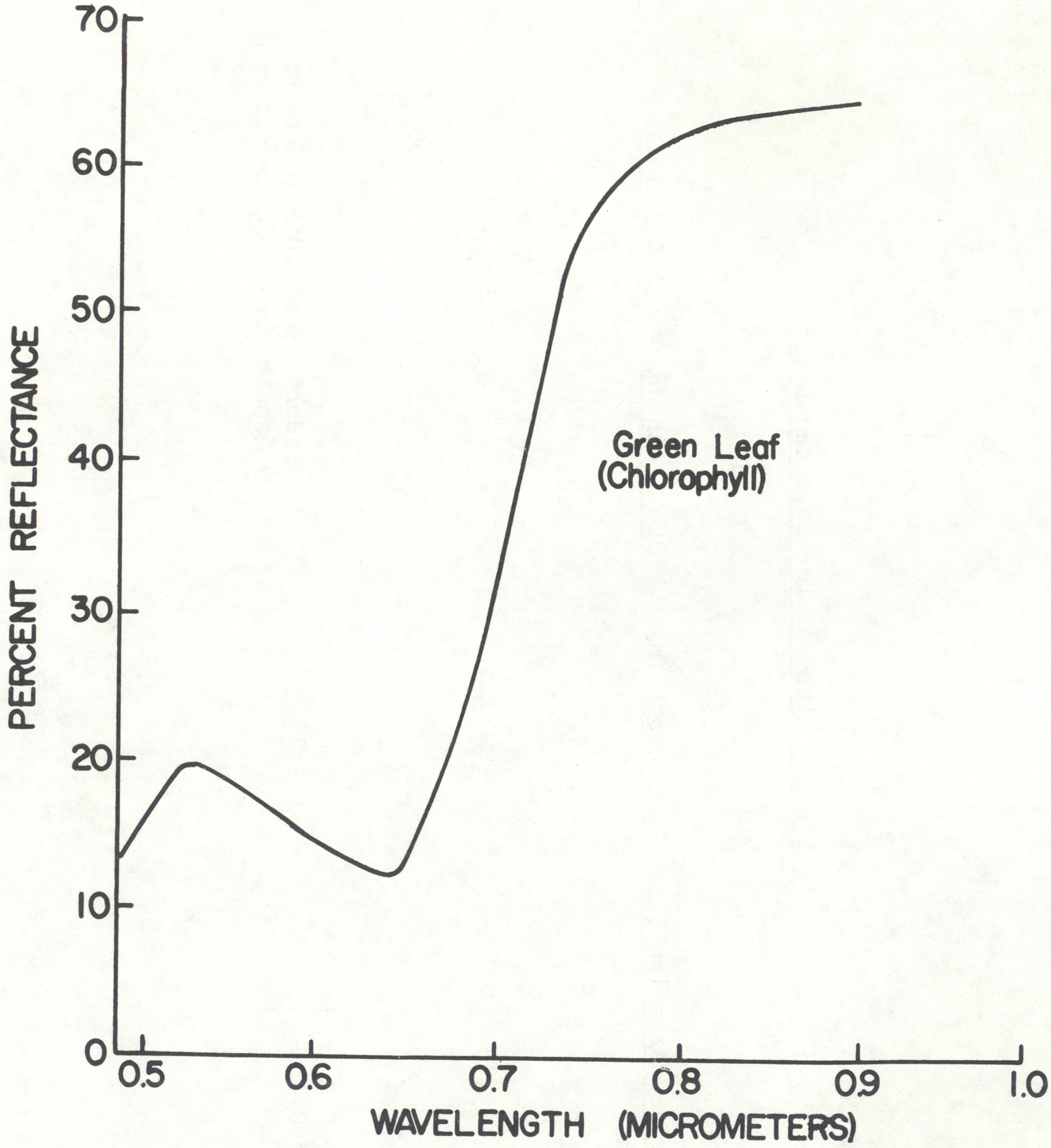

Figure 23 - Spectral response curve for a green leaf (chlorophyll pigment) after Hoffer and Johannsen (1969).

reflectivities, and channel 2- channel 1 disparities, were found over cultivated areas. Figure 24 shows a portion of the May 4th 1980 NOAA-6 image, orbit 4436. Transect L-L on this image is an 80 km W-E line cutting across southern California's fertile Imperial Valley. Figure 25 contains the corresponding channel 1, 2 albedo traces. This valley is irrigated by Colorado River water which is routed thru the All American Canal. Primary crops include sugar beets, cotton and citrus fruits. Imperial Valley has been studied in detail using Landsat MSS images and was the subject of detailed satellite analysis as far back as 1969 when multispectral color photographs of the area were taken by Apollo 9 astronauts (Short et al, 1976). In NOAA-6 visible (channel 1) data Imperial Valley appears very dark and unreflective when compared to the highly reflective desert to the west and east (see Figures 24 and 25). In channel 2 albedoes over the cultivated area increase by almost .20 and can actually be seen to exceed desert brightnesses. Note that the peak channel 2 albedoes coincide with sharp dips in channel 1 albedoes. This conforms to the shape of the green leaf response curve shown in Figure 23. A detailed study of Imperial Valley throughout the 1980 season as viewed from NOAA-6 was the subject of Gatlin et al, 1981.

Figure 26 contains channel 1, 2 albedo traces for another area of cultivation in the southwestern United States. This 50 km W-E profile line is labelled M-M on Figure 24 and consists of irrigated cropland adjacent to the lower Colorado River. Note again the high channel 2 response over the crop area and the paired occurrences of the peak channel 2 albedoes with the lowest channel 1 albedoes. In contrast, reflectivities are almost identical in both channels over the bare desert lying west and east of the fertile valley.

The difference between near-infrared and visible albedoes in areas of active cultivation has been referred to by investigators as the Agricultural Vegetative Index (AVI), Crop Vegetative Index (CVI) and the Green Index Number (GIN). Recent studies have shown that NOAA-6 AVHRR and Landsat MSS vegetative indices were in close agreement when compared over a primary crop growing region along the Brazil-Argentina border (Gray and McCrary, 1981). Figure 27 is a graph from that report showing the AVHRR channel 2-1 vs MSS Band 7-5 relationship. The significant correlation obtained was all the more impressive considering that a) the Landsat MSS data were collected over a three day period (March 15-17, 1980) and the AVHRR data were collected on a single day (March 16, 1980), b) Landsat has an overpass time some two hours later than NOAA-6 (9:20 A.M. vs 7:20 A.M.), and c) Landsat MSS Band 7 and NOAA-6 AVHRR channel 2 differ somewhat in spectral charateristics (see Figure 1). The study shows that NOAA-6 may be able to, at the very least, supplement Landsat as a tool for monitoring world agriculture.

A number of AVHRR channel 2-channel 1 "albedo difference pictures" were created using the H.P. 1000 computer interactive system at the NASA/Goddard Space Flight Center. When color coded, these images provided a quick means of classifying terrain into the following categories: alkali desert, desert shrubland, prairie grassland, forest, (sparse, moderate and dense) and areas under cultivation (light, moderate and intense). Forested regions and cultivated crop lands exhibited similar channel 2-channel 1 difference

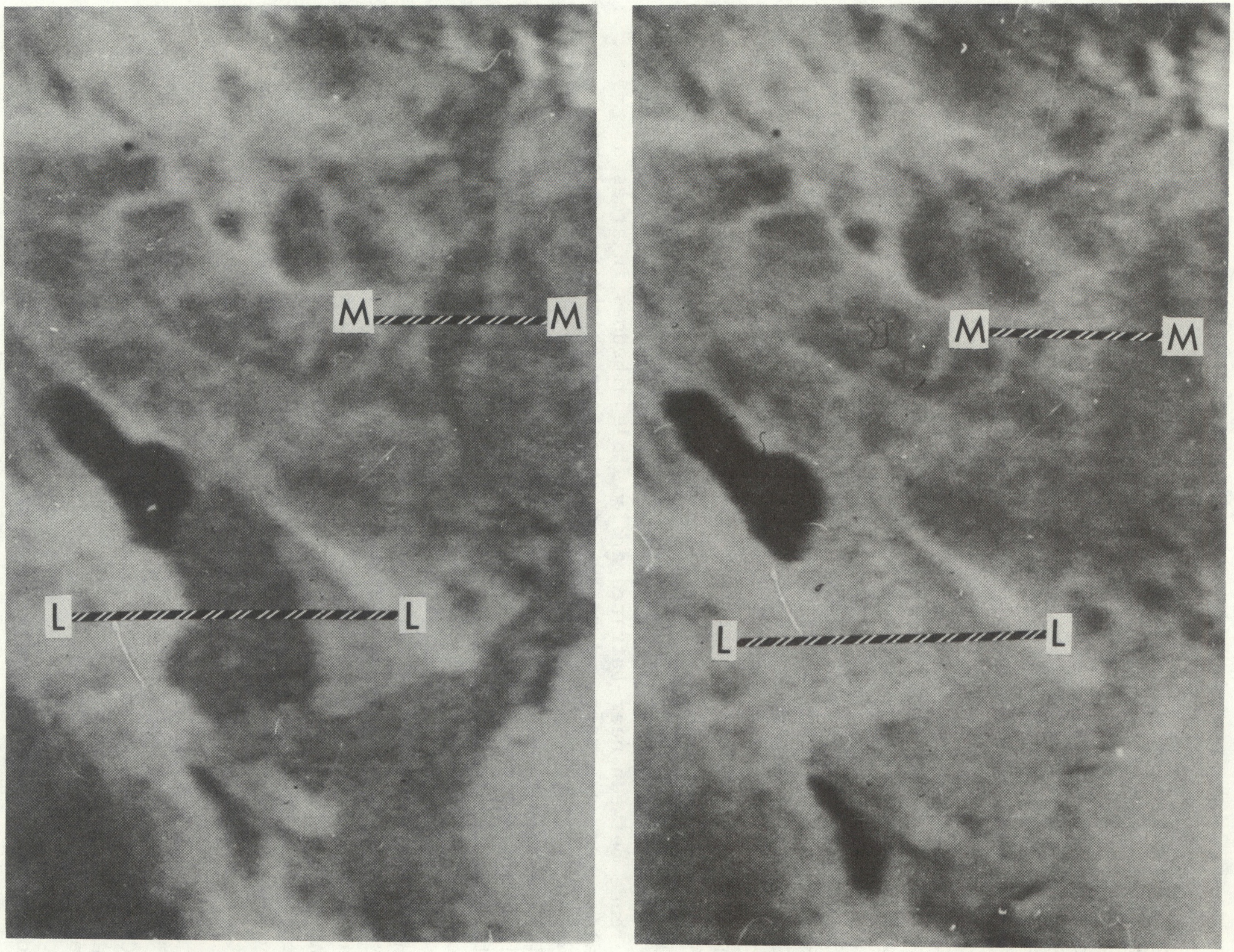

Figure 24 - Visible (left) and near-infrared (right) images of the southern California-Arizona regions. These are blow-ups of the NOAA-6 May 4th, 1980 images, orbit 4436.

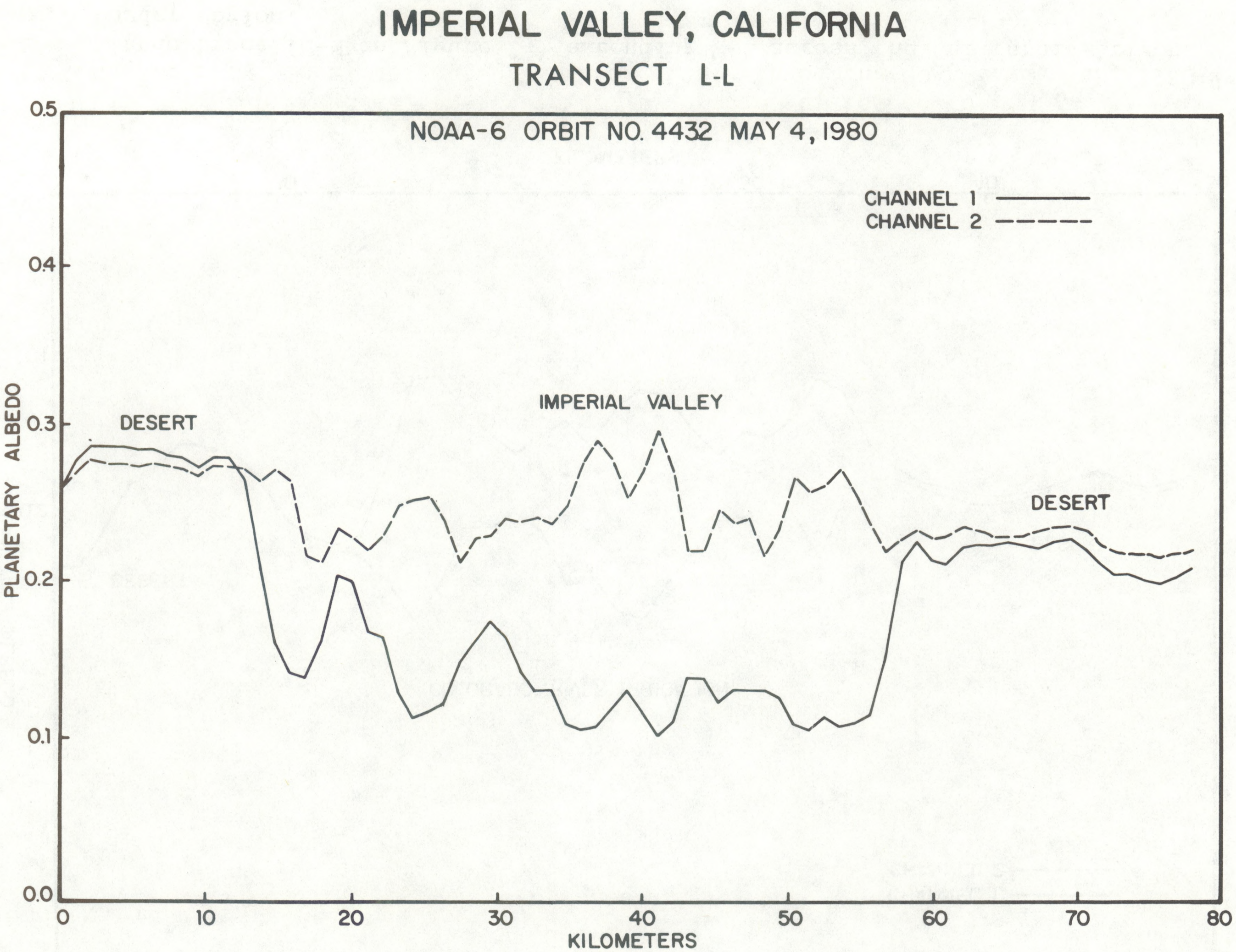

Figure 25 - Albedo trace (L-L on Figure 24) extending W-E across Imperial Valley in Southern California.

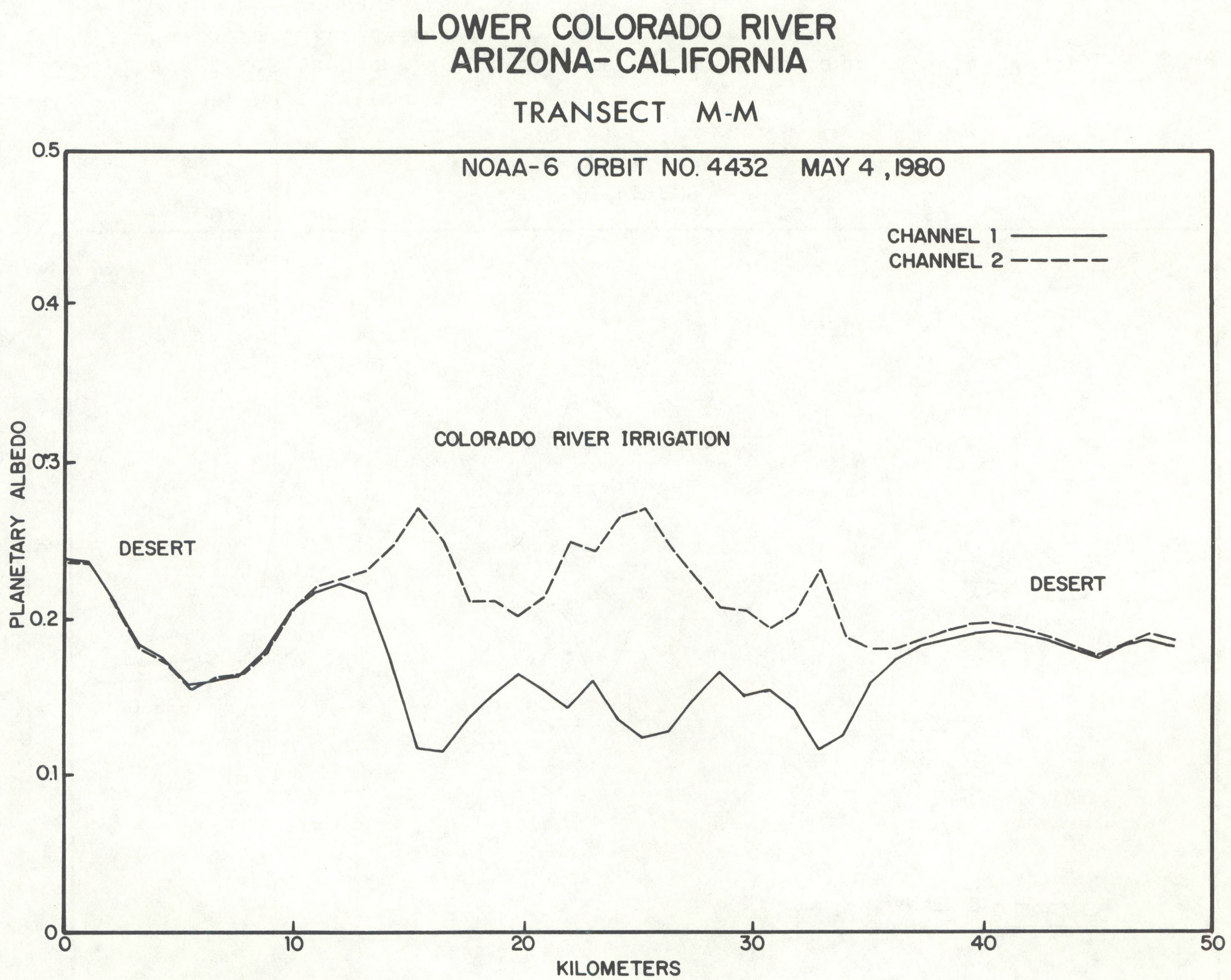

Figure 26 - Albedo trace (M-M on Figure 24) extending W-E across the California-Arizona border region.

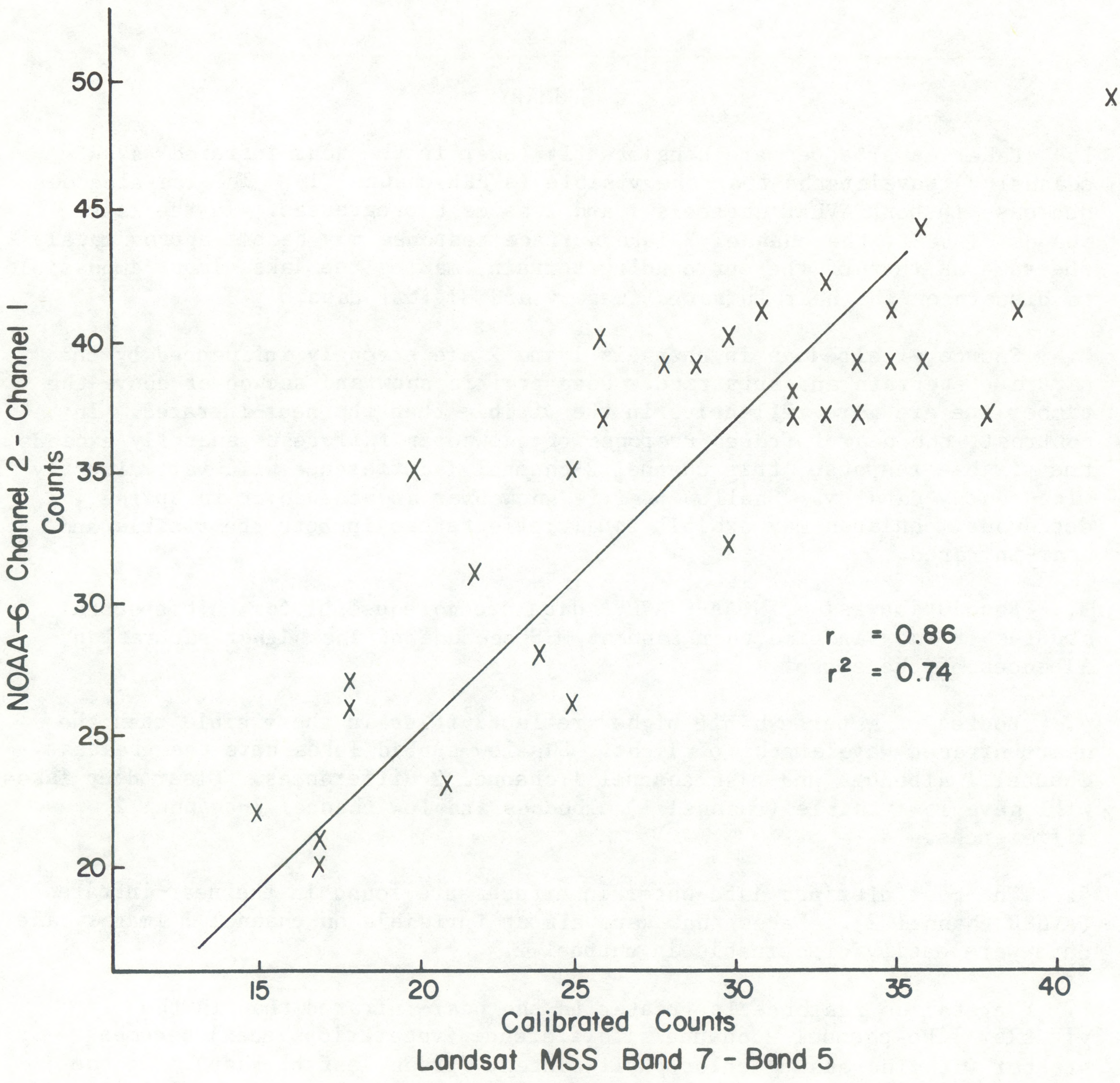

Figure 27 - Significant correlations were found between Landsat MSS Band 7-5 data (horizontal axis) and NOAA-6 AVHRR Channel 2-1 data (vertical axis). The study area was in South America. NOAA-6 data from March 16, 1980. Landsat data from March 15-17, 1980. After Gray and McCrary (1981).

responses and therefore had the same colors on the composited images. The cultivated areas, however, generally could be distinguished from forest by their characteristic geometric patterns.

SUMMARY

1. Lake ice albedoes are consistently lower in the near infrared (AVHRR channel 2) wavelengths than the visible (AVHRR channel 1). The ice albedoes decrease in both AVHRR channels 1 and 2 as melt progresses. In the later stages of melt, the channel 2 lake surface response may become approximately the same as that of the surrounding terrain, making the lake almost impossible to discern on the near infrared imagery and digital data.

2. Snowcover albedoes in channels 1 and 2 are strongly influenced by the nature of terrain and substrate. Deep prairie snow and snowcover above the timberline are more reflective in the visible than the near-infrared. In contrast, the near-infrared response of snowcover in forest generally exceeds the visible response; this channel 2-channel 1 difference will vary directly with canopy density. Shallow prairie snowcover and snowcover in sparse deciduous woodlands may exhibit equal reflectances in both the visible and near-infrared.

3. Resolution aside, NOAA-6 AVHRR data are more useful for multispectral studies of snow and ice than Landsat MSS because of the higher saturation albedoes of the sensor.

4. Bodies of water exhibit higher reflectivities in the visible than the near-infrared wavelengths of light. Shallow turbid lakes have the greatest channel 1 albedoes and high channel 1-channel 2 differences. Clear deep lakes will have low visible (channel 1) albedoes and low channel 1-channel 2 differences.

5. The most distinct land-water interfaces are found in the near-infrared (AVHRR channel 2). Lakes that were almost invisible on channel 1 imagery and data were easily discernable in channel 2.

6. Vegetation response is greater in the near-infrared than in the visible. The channel 2-channel 1 difference (vegetation index) becomes greater with increasing chlorophyll content (green leaf biomass). In the western United States vegetation indices for terrain types were found to ascend in the following order: desert shrubland, prairie grassland, forest, and cultivated crop land.

7. NOAA-6 AVHRR channel 2-channel 1 albedo difference pictures generated on computer interactive systems can be color coded for use in general terrain classification.

REFERENCES

Barnes, J.C., and Smallwood, M.D., 1975: "Synopsis of Current Satellite Snow Mapping Techniques, with Emphasis on the Application of Near-Infrared Data," NASA SP-391, pp. 199-214.

Dozier, J., 1981: Personal Communication, Associate Professor, University of California at Santa Barbara.

Eschner, A. R., Lillesand, T. M., and Meisner, D. E., 1977: "Satellite Remote Sensing of Snowcover in the Adirondack Mountains," Final Report under NOAA Grant No. 04-5-158-43, State University of New York at Syracuse, 86 pp.

Gatlin, J. A., Tucker, C. J., and Schneider, S. R., 1981: "Use of NOAA-6 AVHRR channels one and two for Monitoring Vegetation," Proceedings of the 1981 International Geoscience and Remote Sensing Symposium, Institute of Electrical and Electronics Engineers, New York, New York, abs, in press).

General Electric Corp., 1972: "Data Users Handbook," NASA-Goddard Space Flight Center, Document No. 715D4349.

Gray, T. I. and McCrary D. G., 1981: "Meterological Satellite Data-A Tool to Describe the Health of the World's Agriculture," AgRISTARS Report EW-NI-04042, Johnson Space Center, Houston, Texas, 7pp.

Hoffer, R. M., and Johannsen, C. J., 1969: "Ecological Potential in Spectral Signature Analysis," Remote Sensing in Ecology, University of Georgia Press, Athens, Ga., pp. 1-16.

Holben, B. N., Tucker, C. J., and Fan, C. J., 1980: "Spectral Assessment of Soybean Leaf Area and Leaf Biomass," Photogrammetric Engineering and Remote Sensing, Vol, 46, No. 5, pp. 651-656.

Hussey, J. W., 1977: "The TIROS-N Polar Orbiting Environmental Satellite System," U.S. Department of Commerce, NOAA/NESS, Wash., D.C., 33 pp.

ITT Aerospace/Optical Division, 1980: "Alignment and Calibration Data Book, AVHRR/2," Contract NAS 5-23400, Ft. Wayne, Indiana, 77 pp.

Kidwell, K. B., 1979: "NOAA Polar Orbiter Data, Users Guide," Department of Commerce, National Climatic Center, Satellite Data Services Division, Wash., D.C., 168 pp.

Lin, A., Chang, P., and Sha, P., 1972: "Some Physio-Chemical Characteristics of the Great Salt Lake," In: the Great Salt Lake and Utah's Water Resources, Proceedings of the First Annual Conference of the Utah Section of the American Water Resources Association, pp. 49-65.

Matson, M. and Berg C. P., 1981: "Satellite Detection of Seiches in Great Salt Lake, Utah," Water Resources Bulletin, Vol. 17, No. 1, pp. 122-128.

McGinnis, D. F., 1972: "Satellite Detection of Melting Snow and Ice by Simultaneous Visible and Near-IR Measurements," Proceedings of the Eighth International Symposium on Remote Sensing of Environment, Environmental Research Institute of Michigan, Ann Arbor, Michigan, pp. 231-240.

McGinnis, D. F., 1975: "A Progress Report on Estimating Snow Depth Using VHRR Data from NOAA Environmental Satellite," In Operational Applications of Satellite Snowcover Observations, NASA SP-391, pp. 313-324.

Moore, G. K., 1978: "Satellite Surveillance of Physical Water-Quality Characteristics," Proceedings of the Twelfth International Symposium on Remote Sensing of Environment, Environmental Research Institute of Michigan, Ann Arbor, Michigan, pp. 445-462.

NOAA, 1980: Climatological Data for Colorado, Wyoming, Nebraska and Kansas; Department of Commerce, National Climatic Center, Asheville, North Carolina.

O'Brien, H. W., and Munis, R. H., 1975: "Red and Near-Infrared Spectral Reflectance of Snow," Contract No. NA-869-73, Cold Regions Research and Engineering Laboratory, U. S. Army Corps of Engineers, Hanover, New Hampshire, 18 pp.

Pentland, R. S., 1981: Personal Communication, Hydrology Branch, Saskatchewan Environment, Regina Canada S4P 3V5.

Rango, A., 1980: "Operational Applications of Satellite Snowcover Observations," NASA CP 2116, Goddard Space Flight Center, Greenbelt, MD 301 pp.

Reeves, R.G., 1975: "Manual of Remote Sensing," American Society Photogrammetry, 105 N. Virginia Ave., Falls Church, Va., 22046, p. 80.

Scarpace F. L, and Fisher, L. T., 1980: "The Operational Use of Landsat for Lake Quality Assessment," In: Civil Engineering Applications of Remote Sensing, American Society of Civil Engineers, pp. 88-100.

Schneider, S. R., 1980: "The NOAA/NESS Program for Operational Snowcover Mapping: Preparing for the 1980's," Operational Applications of Satellite Snowcover Observations, NASA CP 2116, Goddard Space Flight Center, Greenbelt, MD, pp. 21-40.

Schwalb, A., 1979: "The TIROS-N/NOAA A-G Satellite Series," Department of Commerce, NOAA Technical Memorandum NESS 95, Wash. D.C., 75 pp.

Short, N. M., Lowman, P. D., Freden, S. C. and Finch, W. A., 1976: "Mission to Earth, Landsat Views the World," NASA SP 360, Goddard Space Flight Center, Greenbelt, MD 459 pp.

Specht, M. R., Needler, D., and Fritz, N. L., 1973: "New Color Film for Water Photography Penetration," Journal of Photogrammetric Engineering, Vol, 39, pp. 359-369.

Strong, A. E., and Eadie, B. J., 1978: "Satellite Observations of Calcium Carbonate Precipitations in the Great Lakes," Journal of Limnology and Oceanography, Vol. 23, No. 5, pp. 877-887.

Sydor, M., 1980: "Remote Sensing of Particulate Concentrations in Water," Journal of Applied Optics, Vol. 19, No. 16, pp. 2794-2800.

Thompson, D. R., and Wehmanen, O. A., 1980: "Using Landsat Digital Data to Detect Moisture Stress in Corn-Soybean Growing Regions," Journal of American Society of Photogrammetry, Vol. 46, No. 8, 00. 1087-1093.

Todd, D. K., 1970: The Water Encyclopedia, Water Research Building, Manhasset Isle, Port Washington, New York, pp. 123-129 and 407-411.

Tucker, C. J., Holben, B. N., Elgin, J. H., and McMurtrey, J. E., 1980 (a): "Remote Sensing of Total Dry-Matter Accumulation in Winter Wheat," NASA Technical Memorandum 80631, Goddard Space Flight Center, 24 pp.

Wiegand, C. L., Richardson, A. J. and Kanemasu, E. T. 1979: "Leaf Area Index Estimates for Wheat from Landsat and their Implications for Evaporation and Crop Modeling," Agron. J. Vol. 71 pp. 336-312.

Wiesnet, D. R., McGinnis, D. F. and McMillan, M. C., 1974: "Evaluation of ERTS Data for Certain Hydrological Uses," Final Report on Contract No. 432-641-14-04-03, NASA Goddard Space Flight Center, Wash. D. C., 88 pp.

Wiesnet, D. R., 1976: "Suspended Sediment in Great Slave Lake, Northwest Territories, Canada," In: ERTS-1, A New Window on Our Planet, U.S. Geological Survey Professional Paper 929, U.S. Government Printing Office Catalog Number I 19. 16:929 pp. 162-163.

APPENDIX A. SATELLITE/ALBEDO CONVERSION TABLES

*** VISIABLE CHANNEL 1 PERCENT ALBETO ***

IMAGE VALUE	PERCENT ALBETO	IMAGE VALUE	PERCENT ALBETO	IMAGE VALUE	PERCENT ALBETO	IMAGE VALUE	PERCENT ALBETO	IMAGE VALUE	PERCENT ALBETO	IMAGE VALUE	PERCENT ALBETO
0	-4.1	43	14.3	86	32.7	129	51.1	172	69.6	215	88.0
1	-3.7	44	14.7	87	33.2	130	51.6	173	70.0	216	88.4
2	-3.3	45	15.2	88	33.6	131	52.0	174	70.4	217	88.8
3	-2.8	46	15.6	89	34.0	132	52.4	175	70.8	218	89.3
4	-2.4	47	16.0	90	34.4	133	52.9	176	71.3	219	89.7
5	-2.0	48	16.4	91	34.9	134	53.3	177	71.7	220	90.1
6	-1.5	49	16.9	92	35.3	135	53.7	178	72.1	221	90.5
7	-1.1	50	17.3	93	35.7	136	54.1	179	72.6	222	91.0
8	-0.7	51	17.7	94	36.2	137	54.6	180	73.0	223	91.4
9	-0.3	52	18.2	95	36.6	138	55.0	181	73.4	224	91.8
10	0.2	53	18.6	96	37.0	139	55.4	182	73.8	225	92.3
11	0.6	54	19.0	97	37.4	140	55.9	183	74.3	226	92.7
12	1.0	55	19.4	98	37.9	141	56.3	184	74.7	227	93.1
13	1.5	56	19.9	99	38.3	142	56.7	185	75.1	228	93.5
14	1.9	57	20.3	100	38.7	143	57.1	186	75.6	229	94.0
15	2.3	58	20.7	101	39.1	144	57.6	187	76.0	230	94.4
16	2.7	59	21.2	102	39.6	145	58.0	188	76.4	231	94.8
17	3.2	60	21.6	103	40.0	146	58.4	189	76.8	232	95.3
18	3.6	61	22.0	104	40.4	147	58.9	190	77.3	233	95.7
19	4.0	62	22.4	105	40.9	148	59.3	191	77.7	234	96.1
20	4.5	63	22.9	106	41.3	149	59.7	192	78.1	235	96.5
21	4.9	64	23.3	107	41.7	150	60.1	193	78.6	236	97.0
22	5.3	65	23.7	108	42.1	151	60.6	194	79.0	237	97.4
23	5.7	66	24.2	109	42.6	152	61.0	195	79.4	238	97.8
24	6.2	67	24.6	110	43.0	153	61.4	196	79.8	239	98.3
25	6.6	68	25.0	111	43.4	154	61.9	197	80.3	240	98.7
26	7.0	69	25.4	112	43.9	155	62.3	198	80.7	241	99.1
27	7.5	70	25.9	113	44.3	156	62.7	199	81.1	242	99.5
28	7.9	71	26.3	114	44.7	157	63.1	200	81.6	243	100.0
29	8.3	72	26.7	115	45.1	158	63.6	201	82.0	244	100.4
30	8.7	73	27.2	116	45.6	159	64.0	202	82.4	245	100.8
31	9.2	74	27.6	117	46.0	160	64.4	203	82.8	246	101.3
32	9.6	75	28.0	118	46.4	161	64.8	204	83.3	247	101.7
33	10.0	76	28.4	119	46.9	162	65.3	205	83.7	248	102.1
34	10.5	77	28.9	120	47.3	163	65.7	206	84.1	249	102.5
35	10.9	78	29.3	121	47.7	164	66.1	207	84.6	250	103.0
36	11.3	79	29.7	122	48.1	165	66.6	208	85.0	251	103.4
37	11.7	80	30.2	123	48.6	166	67.0	209	85.4	252	103.8
38	12.2	81	30.6	124	49.0	167	67.4	210	85.8	253	104.3
39	12.6	82	31.0	125	49.4	168	67.8	211	86.3	254	104.7
40	13.0	83	31.4	126	49.9	169	68.3	212	86.7	255	105.1
41	13.4	84	31.9	127	50.3	170	68.7	213	87.1		
42	13.9	85	32.3	128	50.7	171	69.1	214	87.6		

Figure A-1 NOAA-6 AVHRR Channel 1 look-up table showing 8 bit satellite digital count values vs. albedoes.

*** VISIABLE CHANNEL 2 PERCENT ALBETO ***

IMAGE VALUE	PERCENT ALBETO	IMAGE VALUE	PERCENT ALBETO	IMAGE VALUE	PERCENT ALBETO	IMAGE VALUE	PERCENT ALBETO	IMAGE VALUE	PERCENT ALBETO	IMAGE VALUE	PERCENT ALBETO
0	-3.5	43	14.7	86	32.9	129	51.1	172	69.3	215	87.5
1	-3.0	44	15.2	87	33.4	130	51.5	173	69.7	216	87.9
2	-2.6	45	15.6	88	33.8	131	52.0	174	70.2	217	88.4
3	-2.2	46	16.0	89	34.2	132	52.4	175	70.6	218	88.8
4	-1.8	47	16.4	90	34.6	133	52.8	176	71.0	219	89.2
5	-1.3	48	16.9	91	35.0	134	53.2	177	71.4	220	89.6
6	-0.9	49	17.3	92	35.5	135	53.7	178	71.9	221	90.1
7	-0.5	50	17.7	93	35.9	136	54.1	179	72.3	222	90.5
8	-0.1	51	18.1	94	36.3	137	54.5	180	72.7	223	90.9
9	0.4	52	18.5	95	36.7	138	54.9	181	73.1	224	91.3
10	0.8	53	19.0	96	37.2	139	55.4	182	73.5	225	91.7
11	1.2	54	19.4	97	37.6	140	55.8	183	74.0	226	92.2
12	1.6	55	19.8	98	38.0	141	56.2	184	74.4	227	92.6
13	2.0	56	20.2	99	38.4	142	56.6	185	74.8	228	93.0
14	2.5	57	20.7	100	38.9	143	57.0	186	75.2	229	93.4
15	2.9	58	21.1	101	39.3	144	57.5	187	75.7	230	93.9
16	3.3	59	21.5	102	39.7	145	57.9	188	76.1	231	94.3
17	3.7	60	21.9	103	40.1	146	58.3	189	76.5	232	94.7
18	4.2	61	22.4	104	40.5	147	58.7	190	76.9	233	95.1
19	4.6	62	22.8	105	41.0	148	59.2	191	77.4	234	95.6
20	5.0	63	23.2	106	41.4	149	59.6	192	77.8	235	96.0
21	5.4	64	23.6	107	41.8	150	60.0	193	78.2	236	96.4
22	5.9	65	24.0	108	42.2	151	60.4	194	78.6	237	96.8
23	6.3	66	24.5	109	42.7	152	60.9	195	79.0	238	97.2
24	6.7	67	24.9	110	43.1	153	61.3	196	79.5	239	97.7
25	7.1	68	25.3	111	43.5	154	61.7	197	79.9	240	98.1
26	7.5	69	25.7	112	43.9	155	62.1	198	80.3	241	98.5
27	8.0	70	26.2	113	44.4	156	62.5	199	80.7	242	98.9
28	8.4	71	26.6	114	44.8	157	63.0	200	81.2	243	99.4
29	8.8	72	27.0	115	45.2	158	63.4	201	81.6	244	99.8
30	9.2	73	27.4	116	45.6	159	63.8	202	82.0	245	100.2
31	9.7	74	27.9	117	46.0	160	64.2	203	82.4	246	100.6
32	10.1	75	28.3	118	46.5	161	64.7	204	82.9	247	101.1
33	10.5	76	28.7	119	46.9	162	65.1	205	83.3	248	101.5
34	10.9	77	29.1	120	47.3	163	65.5	206	83.7	249	101.9
35	11.4	78	29.5	121	47.7	164	65.9	207	84.1	250	102.3
36	11.8	79	30.0	122	48.2	165	66.4	208	84.6	251	102.7
37	12.2	80	30.4	123	48.6	166	66.8	209	85.0	252	103.2
38	12.6	81	30.8	124	49.0	167	67.2	210	85.4	253	103.6
39	13.0	82	31.2	125	49.4	168	67.6	211	85.8	254	104.0
40	13.5	83	31.7	126	49.9	169	68.0	212	86.2	255	104.4
41	13.9	84	32.1	127	50.3	170	68.5	213	86.7		
42	14.3	85	32.5	128	50.7	171	68.9	214	87.1		

Figure A-2 NOAA-6 AVHRR Channel 2 look-up table showing 8 bit satellite digital count values vs. albedoes

APPENDIX B. H.P. 1000 SYSTEM SCHEMATIC

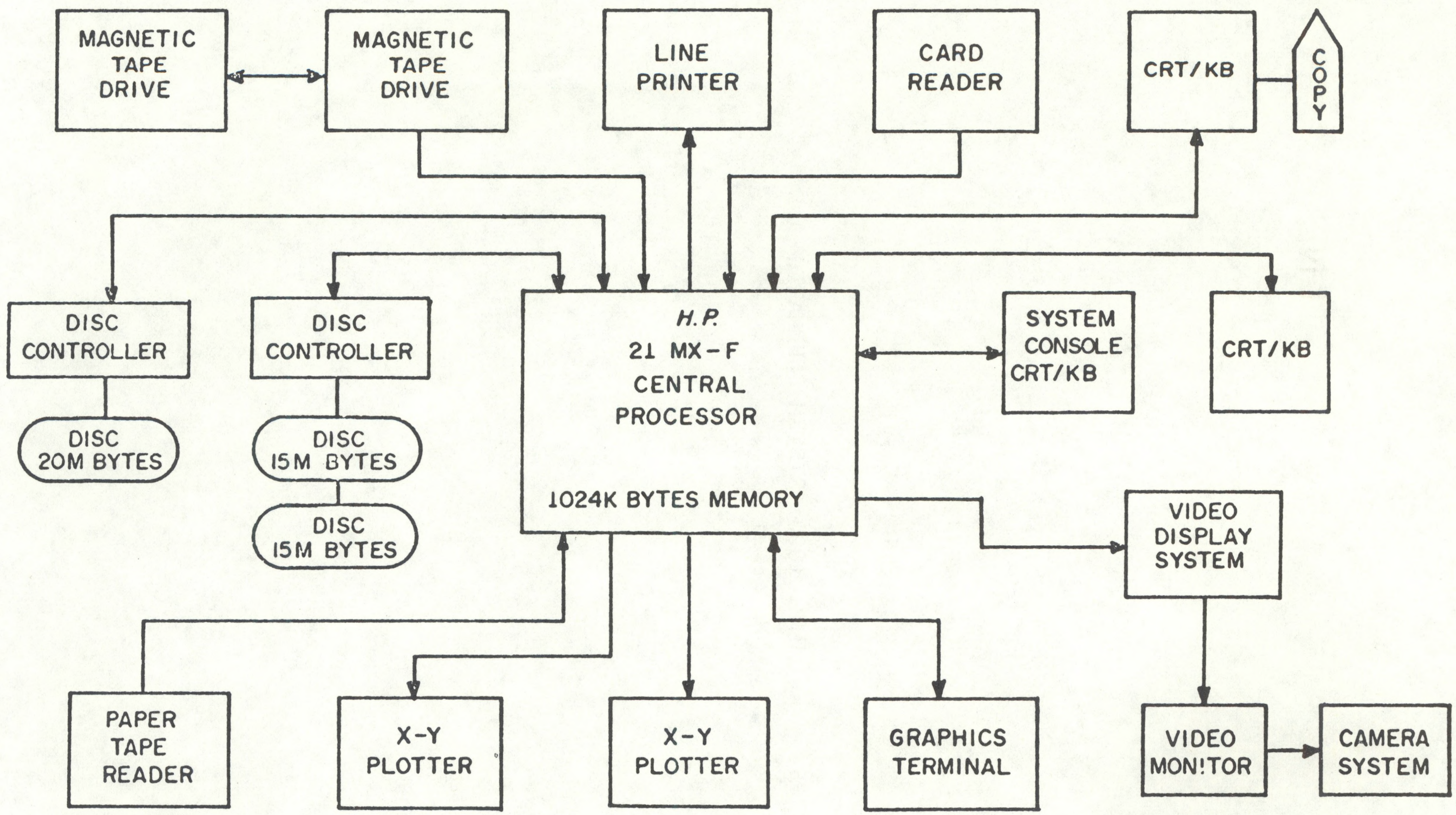

H.P. 1000 SYSTEM

NASA GODDARD

EARTH OBSERVATION SYSTEMS DIVISION

Figure B-1 Schematic of the H.P. 1000 computer interactive system used for analyzing the AVHRR data in this report.

(Continued from inside front cover)

NESS 61 The Measurement of Atmospheric Transmittance From Sun and Sky With an Infrared Vertical Sounder. W. L. Smith and H. B. Howell, September 1972, 16 pp. (COM-73-50020)

NESS 62 Proposed Calibration Target for the Visible Channel of a Satellite Radiometer. K. L. Coulson and H. Jacobowitz, October 1972, 27 pp. (COM-73-10143)

NESS 63 Verification of Operational SIRS B Temperature Retrievals. Harold J. Brodrick and Christopher M. Hayden, December 1972, 26 pp. (COM-73-50279)

NESS 64 Radiometric Techniques for Observing the Atmosphere From Aircraft. William L. Smith and Warren J. Jacob, January 1973, 12 pp. (COM-73-50376)

NESS 65 Satellite Infrared Soundings From NOAA Spacecraft. L. M. McMillin, D. Q. Wark, J.M. Siomkajlo, P. G. Abel, A. Werbowetzki, L. A. Lauritson, J. A. Pritchard, D. S. Crosby, H. M. Woolf, R. C. Luebbe, M. P. Weinreb, H. E. Fleming, F. E. Bittner, and C. M. Hayden, September 1973, 112 pp. (COM-73-50936/6AS)

NESS 66 Effects of Aerosols on the Determination of the Temperature of the Earth's Surface From Radiance Measurements at 11.2 m. H. Jacobowitz and K. L. Coulson, September 1973, 18 pp. (COM-74-50013)

NESS 67 Vertical Resolution of Temperature Profiles for High Resolution Infrared Radiation Sounder (HIRS). Y. M. Chen, H. M. Woolf, and W. L. Smith, January 1974, 14 pp. (COM-74-50230)

NESS 68 Dependence of Antenna Temperature on the Polarization of Emitted Radiation for a Scanning Microwave Radiometer. Norman C. Grody, January 1974, 11 pp. (COM-74-50431/AS)

NESS 69 An Evaluation of May 1971 Satellite-Derived Sea Surface Temperatures for the Southern Hemisphere. P. Krishna Rao, April 1974, 13 pp. (COM-74-50643/AS)

NESS 70 Compatibility of Low-Cloud Vectors and Rawins for Synoptic Scale Analysis. L. F. Hubert and L. F. Whitney, Jr., October 1974, 26 pp. (COM-75-50065/AS)

NESS 71 An Intercomparison of Meteorological Parameters Derived From Radiosonde and Satellite Vertical Temperature Cross Sections. W. L. Smith and H. M. Woolf, November 1974, 13 pp. (COM-75-10432)

NESS 72 An Intercomparison of Radiosonde and Satellite-Derived Cross Sections During the AMTEX. W. C. Shen, W. L. Smith, and H. M. Woolf, February 1975, 18 pp. (COM-75-10439/AS)

NESS 73 Evaluation of a Balanced 300-mb Height Analysis as a Reference Level for Satellite-Derived soundings. Albert Thomasell, Jr., December 1975, 25 pp. (PB-253-058)

NESS 74 On the Estimation of Areal Windspeed Distribution in Tropical Cyclones With the Use of Satellite Data. Andrew Timchalk, August 1976, 41 pp. (PB-261-971)

NESS 75 Guide for Designing RF Ground Receiving Stations for TIROS-N. John R. Schneider, December 1976, 126 pp. (PB-262-931)

NESS 76 Determination of the Earth-Atmosphere Radiation Budget from NOAA Satellite Data. Arnold Gruber, November 1977, 31 pp. (PB-279-633)

NESS 77 Wind Analysis by Conditional Relaxation. Albert Thomasell, Jr., January 1979.

NESS 78 Geostationary Operational Environmental Satellite/Data Collection System. July 1979, 86 pp. (PB-301-276)

NESS 79 Error Characteristics of Satellite-Derived Winds. Lester F. Hubert and Albert Thomasell, Jr. June 1979, 44 pp. (PB-300-754)

NESS 80 Calculation of Atmospheric Radiances and Brightness Temperatures in Infrared Window Channels of Satellite Radiometers. Michael P. Weinreb and Michael L. Hill, March 1980, 43 pp. (PB80 208-119)

NESS 81 Improved Algorithm for Calculation of UTM and Geodetic Coordinates. Jeff Dozier, September 1980, 21 pp. (PB81 132680)

NESS 82 The Effect of Precipitation on Microwave Soundings in Low Latitudes. Lester F. Hubert, Norman C. Grody, Andrew Timchalk, and William C. Shen, April 1981, 34 pp. (PB81 225062)

NESS 83 Atmospheric Sounding User's Guide. Adolf Werbowetzki, ed., April 1981, 82 pp. (PB81 230476)

NOAA SCIENTIFIC AND TECHNICAL PUBLICATIONS

The National Oceanic and Atmospheric Administration was established as part of the Departmen Commerce on October 3, 1970. The mission responsibilities of NOAA are to assess the socioeconomic im of natural and technological changes in the environment and to monitor and predict the state of the solid Earth, the oceans and their living resources, the atmosphere, and the space environment of the Earth.

The major components of NOAA regularly produce various types of scientific and technical information in the following kinds of publications:

PROFESSIONAL PAPERS — Important definitive research results, major techniques, and special investigations.

CONTRACT AND GRANT REPORTS — Reports prepared by contractors or grantees under NOAA sponsorship.

ATLAS — Presentation of analyzed data generally in the form of maps showing distribution of rainfall, chemical and physical conditions of oceans and atmosphere, distribution of fishes and marine mammals, ionospheric conditions, etc.

TECHNICAL SERVICE PUBLICATIONS — Reports containing data, observations, instructions, etc. A partial listing includes data serials; prediction and outlook periodicals; technical manuals, training papers, planning reports, and information serials; and miscellaneous technical publications.

TECHNICAL REPORTS — Journal quality with extensive details, mathematical developments, or data listings.

TECHNICAL MEMORANDUMS — Reports of preliminary, partial, or negative research or technology results, interim instructions, and the like.

NATIONAL OCEANIC AND ATMOSPHERIC ADMINISTRATION
NOAA
U.S. DEPARTMENT OF COMMERCE

Information on availability of NOAA publications can be obtained from:

ENVIRONMENTAL SCIENCE INFORMATION CENTER (D822)
ENVIRONMENTAL DATA AND INFORMATION SERVICE
NATIONAL OCEANIC AND ATMOSPHERIC ADMINISTRATION
U.S. DEPARTMENT OF COMMERCE

6009 Executive Boulevard
Rockville, MD 20852

NOAA--S/T 81-188